NUMERICAL VALIDATION OF A ROBUST POSITIONING CONTROLLER IN MACHINE TOOLS APPLICATION

Submitted by

Vepouyoum Njouokouo Youssef
190011138

Aminu Muhammad Mukaddas
190011136

Abdul Malek Thabet Naji
190011137

Mohammed K A Rook
180011251

Supervised by

Dr. Madihah binti Haji Maharof

A Thesis submitted in partial fulfillment of the requirement of the degree of Bachelor of Science in Mechanical Engineering

Department of Mechanical and Production Engineering (MPE)

Islamic University of Technology (IUT)

June, 2024

Candidate's Declaration

This is to certify that the work presented in this thesis, "NUMERICAL VALIDATION OF A ROBUST POSITIONING CONTROLLER IN MACHINE TOOLS APPLICATION", is the outcome of the investigation and research carried out by Vepouyoum Njouokouo Youssef (190011138), Abdul Malek Thabet Naji (190011137), Aminu Muhammad Mukaddas (190011136) and Mohammed K A Rook (180011251) under the supervision of Dr. Madihah binti Haji Maharof, Asistant Professor, MPE, IUT in the year 2024.

It is also declared that neither this thesis nor any part of it had been submitted elsewhere for the award of any degree or diploma.

Vepouyoum Njouokouo Youssef
190011138

Abdul Malek Thabet Naji
190011137

Aminu Muhammad Mukaddas
190011136

Mohammed K A Rook
1800111251

Recommendation of the Thesis Supervisors

This thesis titled "NUMERICAL VALIDATION OF A ROBUST POSITIONING CONTROLLER IN MACHINE TOOLS APPLICATION" submitted by VEPOUYOUM NJOUOKOUO YOUSSEF (190011138), ABDUL MALEK THABET NAJI (190011137), AMINU MUHAMMAD MUKADDAS (190011136) and MOHAMMED K A ROOK (180011251) has been accepted as satisfactory in partial fulfillment of the requirement for the Degree of Bachelor of Science in Mechanical Engineering **on 22nd June, 2024**

Supervisor

Dr. Madihah binti Haji Maharof
Assistant Professor
MPE Dept., IUT Board Bazar, Gazipur-1704, Bangladesh.

Head of Department

Prof. Dr. Md. Hamidur Rahman
Professor
MPE Dept., IUT Board Bazar, Gazipur-1704, Bangladesh.

Department of Mechanical and Production Engineering (MPE)
Islamic University of Technology (IUT)

CO-PO Mapping of ME 4800 - Thesis and Project

COs	Course Outcomes (CO) Statement	(PO)	Addressed by	
CO1	Discover and Locate research problems and illustrate them via figures/tables or projections/ideas through field visit and literature review and determine/Setting aim and objectives of the project/work/research in specific, measurable, achievable, realistic and timeframe manner.	**PO2**	Thesis Book	
			Performance by research	
			Presentation and soft skill	
CO2	Design research solutions of the problems towards achieving the objectives and its application. Design systems, components or processes that meets related needs in the field of mechanical engineering	**PO3**	Thesis Book	
			Performance by research	
			Presentation and soft skill	
CO3	Review, debate, compare and contrast the relevant literature contents. Relevance of this research/study. Methods, tools, and techniques used by past researchers and justification of use of them in this work.	**PO4**	Thesis Book	
			Performance by research	
			Presentation and soft skill	
CO4	Analyze data and exhibit results using tables, diagrams, graphs with their interpretation. Investigate the designed solutions to solve the problems through case study/survey study/experimentation/simulation using modern tools and techniques.	**PO5**	Thesis Book	
			Performance by research	
			Presentation and soft skill	
CO5	Apply outcome of the study to assess societal, health, safety, legal and cultural issue and consequent possibilities relevant to mechanical engineering practice.	**PO6**	Thesis Book	
			Performance by research	
			Presentation and soft skill	
CO6	Relate the solution/s to objectives of the research/work for improving desired performances including economic, social and environmental benefits.	**PO7**	Thesis Book	
			Performance by research	
			Presentation and soft skill	
CO7	Apply moral values and research/professional ethics throughout the work, and justify to genuine referencing on sources, and demonstration of own contribution.	**PO8**	Thesis Book	
			Performance by research	
			Presentation and soft skill	
CO8	Perform own self and manage group activities from the beginning to the end of the research/work as a quality work.	**PO9**	Thesis Book	
			Performance by research	
			Presentation and soft skill	
CO9	Compile and arrange the work outputs, write the report/thesis, a sample journal paper, and present the work to wider audience using modern communication tools and techniques.	**PO10**	Thesis Book	
			Performance by research	
			Presentation and soft skill	
CO10	Organize and control cost and time of the work/project/research and coordinate them until the end of it.	**PO11**	Thesis Book	
			Performance by research	
			Presentation and soft skill	
CO11	Recognize the necessity of life-long learning in career development in dynamic real-world situations from the experience of completing this project.	**PO12**	Thesis Book	
			Performance by research	
			Presentation and soft skill	

K-P-A Mapping of ME 4800 -Thesis and Project

COs	POs	Related Ks								Related Ps							Related As				
		K1	K2	K3	K4	K5	K6	K7	K8	P1	P2	P3	P4	P5	P6	P7	A1	A2	A3	A4	A5
CO1	PO2																				
CO2	PO3																				
CO3	PO4																				
CO4	PO5																				
CO5	PO6																				
CO6	PO6																				
CO7	PO8																				
CO8	PO9																				
CO9	PO10																				
CO10	PO11																				
CO11	PO12																				

Student Name /ID:

1. .....

2. .....

3. .....

4. .....

Signature of the Supervisor:

.....

Name of the Supervisor:

.....

ABSTRACT

Cutting force and friction force are two disturbance forces that directly affect the servo drive system during the milling process, causing a negative effect that reduces the positioning table's precision. To maintain the final product's quality and geometric precision, this influence must be countered. The main goal of this thesis is to reduce the disturbance by designing effective controllers to compensate for these injected disturbance forces at a spindle speed of 1500 rpm. This thesis proposes PID, Cascade P/PI and Sliding Mode Control (SMC), with its modified structures Sigmoid SMC and SuperTwisting SMC (ST-SMC). The PID and cascade was designed using conventional loop shaping method, while SMC was design using its traditional formulation and heuristic tuning methods. The numerical analysis was performed using MATLAB/Simulink software and performance was tested using performance index; Maximum Tracking Error (MTE), Root Mean Square Error (RMSE) and Fast Fourier Transform (FFT). The results obtained showed that Sigmoid SMC controller produced superior performance over the others. With Maximum Tracking error showed that Sigmoid SMC produced the best tracking error with percentage reduction of 85 % on reference to Cascade P/PI with highest tracking error. In terms of RMSE, PID produced the most percentage variation error of 45.9 % while cascade had the lowest of 2.70 %. In regards to the FFT results, the Sigmoid SMC showed the most reduction of peak amplitude of 68.3 % and PID showed the lowest peak reduction of 19.4 %. The chattering phenomenon in SMC is addressed by modifying the classical SMC, and the numerical analysis displayed a robust SMC to compensate disturbance forces while reducing chattering effect.

Keywords: Cutting force, Disturbance forces, Robust control, Tracking error, Controller design, Disturbance compensation.

ACKNOWLEDGEMENTS

In the Name of Allah, the Most Gracious, the Most Merciful

We first of all thank the Almighty, creator of the sky and heavens. Words cannot express our gratitude to our supervisor Dr. Madihah Binti Haji Maharof for her invaluable support, teachings, patience and feedback. We also could not have undertaken this journey without her, who generously provided knowledge and expertise in her domain. Additionally, this endeavor would not have been possible without the approval of Prof. Dr. Md. Anayet Ullah Patwari.

We are also grateful to a very important person that has indirectly contributed to this achievement, Prof. Dr. Zamberi Bin Jamaludin. who finely thought us Control theory for one semester providing us a benchmark for this thesis. His goodness will not be forgotten.

Our heartfelt thanks go to our fellow group members, Vepouyoum Youssef, Aminu Mukaddas, AbdulMalek Thabit, Mouhammed Rook for their collaborative spirit, hard work, and commitment to excellence. Each member has played a vital role in contributing to different aspects of the research, from data collection and analysis to writing and editing.

Lastly, We would be remiss in not mentioning our families, especially our parents, brothers, and sisters. Their belief in us has kept our spirits and motivation high during this process. We would also like to thank the Mamas of all IUT campus for the unseen help they provide in every day to day activities.

TABLE OF CONTENTS

LIST OF FIGURES

LIST OF TABLES

LIST OF ABBREVIATIONS

3D	Three Dimensional
CAD	Computer Aided Design
CAM	Computer Aided Manufacturing
CNC	Computer Numerical Control
CP	Continuous Path
DoF	Degree of Freedom
DSP	Digital Signal Processing
FFT	Fast Fourier Transform
GM	Gain Margin
I/O	Input/Output
MTE	Maximum Tracking Error
P	Proportional
PI	Proportional-Integral
PID	Proportional-Integral-Derivative
PM	Phase Margin
PTP	Point-to-Point
RPM	Rotation Per Minute
RSME	Root Mean Square Error
SISO	Single-Input Single-Output
SMC	Sliding Mode Control
ST-SMC	Super Twisted Sliding Mode Control

LIST OF SYMBOLS

K_p	Proportional gain
K_i	Integral gain
K_d	Derivative gain
K_t	Motor constant
T_s	Settling time
T_r	Rise time
T_p	Peak time
T_d	Time delay
e_{ss}	Steady-state error
$e(t)$	Error signal
$e_{vel}(t)$	Velocity error signal
$n(t)$	Noise signal
$d(t)$	External disturbance
$y(t)$	Output signal
$r(t)$	Reference input signal
V	Cutting speed
π	Pi
D	Diameter of Cutter
N	Spindle rotational speed
f	Feed per tooth
nn	Number of cutter's teeth
$L(s)$	Open loop transfer function
$T(s)$	Closed loop transfer function
$S(s)$	Sensitivity transfer function
$R(s)$	Reference position
$Y(s)$	Actual position

ζ	Damping ratio
δ	Degree of continuous approximation
λ	Positive constant
K	CLassical Sliding Control gain

Chapter 1

INTRODUCTION

1.1 Introduction

Achieving precise and consistent placement in manufacturing industries is crucial when it comes to precision machining and production process. The effectiveness of the controller in use is crucial for the accurate control of machining operations, especially in Computer Numerical Control (CNC) systems. CNC machines which can vary from different sizes, number of axes, workspaces and many other characteristics. For CNC machining processes to achieve the requisite positioning accuracy, traditional control approaches have proven crucial. To maintain maximum accuracy and efficiency, it is essential to systematically assess and monitor the performance of these traditional controllers as production demands continue to change.

Classical controllers are control algorithms that are based on well-known control theories, such as Proportional-Integral-Derivative (PID) and cascade P/PI control, which is frequently used in a variety of industrial processes, including CNC machining. Such controllers' main objective is to govern a system's behavior in order to provide desired output characteristics. The controller's job in precision machining is to place the cutting tool and workpiece precisely so that the finished product has exact and repeatable specifications.

1.2 Problem Statement

Precision placement in CNC machining always arises with difficulties, though. Cutting forces and friction within the machining system are a significant barrier. The forces produced by the cutting tool when it interacts with the workpiece can cause vibration, chatter, and even material deformation in the process. In high-speed machining and complex geometries, where the cutting forces can fluctuate greatly, these effects are particularly noticeable.

The issue is made worse by friction at numerous interfaces, including tool-workpiece contact points and mechanical parts. Unmanaged friction can add uncertainty into the positioning process, causing detours from the intended course and compromising the dimensional precision of the finished product. Additionally, the accumulation of friction-induced wear over time may shorten the useful life of an item and necessitate more frequent repair.

The origin of cutting force arises during the machining process, the interaction between the material of the workpiece and the cutting tool produces the majority of

the cutting forces. The strength and direction of these forces are greatly influenced by elements such tool geometry, material characteristics, cutting speed, and feed rate. On the other hand, friction results from the interaction of moving components within the machine, such as bearings, ball screws, and linear guides.

1.3 Objectives

1. To design a controller to compensate for the input disturbances during milling processes using classical cascade P/PI and Proportional-Integral-Derivative(PID), Sliding Mode Control (SMC).

2. To validate numerically the control performance of the designed controller.

1.4 Scopes

1. Numerical validation and control design using MATLAB/Simulink Software

2. Implementation of classical cascade P/PI, as well as Proportional-Integral-Derivative (PID) controller, Sliding Mode Control (SMC).

3. Evaluation of tracking performance using Maximum Tracking Error (MTE), Root Mean Square Error (RMSE), Fast Fourier Transform (FFT).

Chapter 2

LITERATURE REVIEW

2.1 Background

Through out the era of manufacturing, Machine tools comprises of removing material from a work piece in order to produce a required product; these processes include milling, grinding, turning etc. Developing these machine tools directly rely on the advent of tougher work materials, demand of surface quality, a trend on higher component accuracy, higher growth of automation processes and many more. These fast-growing demands directly impacts on researchers and machine tools manufacturers, forcing them to develop new technologies in order to meet these performances. In the last decade, great amount of work has been put in the elimination of imprecisions on machine tools where manufacturers achieve accuracies of 0.005mm [Ramesh et al., 2000].

2.2 Mechanical Drive Systems

In mechatronics systems, mechanical drive systems are widely used in order to transmit motion from one point to another. In machine tools applications, the workpiece and cutting tool are mounted on the feed drive which are moved and positioned in the desired location. The development of high-speed and precise motion system have grown over the past decade, thus developing precise control algorithm are necessary to effectively compensate for the disturbances generated by this motion systems. Various feed-drives are powered either by direct linear motor or by rotary motors via a mechanism to transmit power. The most fundamentally encountered used feed-drives include;- (*i*) Rack-pinion-drive, (*ii*) Ballscrew (*iii*) Linear direct drives. [Altintas et al., 2011]

2.2.1 Rack-pinion drive

A classic Rack and pinion system as shown in Figure 2.1, typically consist of a pinion, driven by a motor attached to a gearbox that mates with a linear gear called rack. Rack and pinion drives are used in applications where the machine is heavy and has extended feed travel. However, designing a rack and pinion drive system is highly dependent on it's torsional stiffness and clearance between the mating teeth. A free of clearance rack and pinion drive reduces vibration and positioning error; thus, improving the tracking performance of the whole machine. To design a clearance free feed drive, Sawicki et al. [Sawicki, 2021] proposes to use two pinions

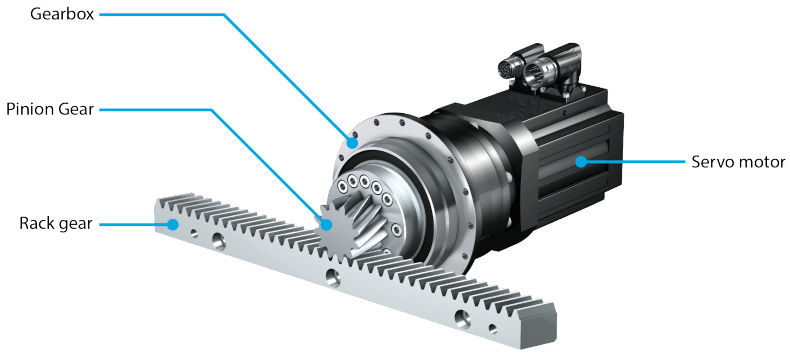

Figure 2.1: *Rack and pinion drive system*

with motors rotating in opposite direction; that is, the main motor applies high torque to delivery the motion and the second motor delivers less torque to remove the clearance. This ensures a continuous contact between the teeth, regardless of the direction of the motion.

2.2.2 Linear direct drive

A linear drive is a synchronous brushless motor servo that operates on electrodynamics principle. In linear drives, the load moves without any mechanical power conversion. It consist of a lamination stacks, magnet and coil as shown in Figure 2.1. It is comprised of a primary part - stator, a secondary part - permanent magnet.

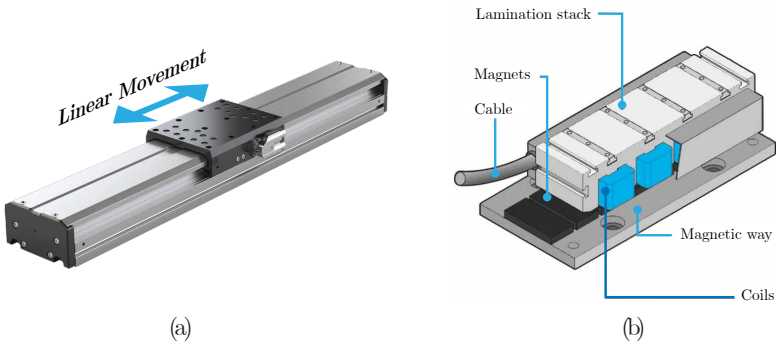

Figure 2.2: *(a) Linear motor stage (b) Iron core structure (reproduced from, www.etel.ch)*

The force generated by the motor coil is directly connected to the load. The motor coil propels itself on a magnetic track and is attached to the carriage with

the load bolted directly to it. The carriage is hold in place by linear bearings, with rails secured to the base. There is a small air spacing between the motor coil and magnet track and the position of the carriage is reported by a linear encoder. In exclusion of nuts, couplers and screws, linear motor drives provides fast acceleration, rapid positioning and high feed rates.

2.2.3 Ball screw drive

The most common feed system with drives used in machining applications is ball screw drive as shown in Figure 2.3. The system driven by a ball screw is used in electromechanical systems. Since the machined pieces are exposed to a lot of heat, there is a risk to their accuracy due to the increased positioning errors due to the driven system. The key function of the ball screw is the transmission system structure is great precision. It converts the rotating motion of the motor into linear motion. Furthermore, the ball screw-driven system can be sized to fit different spaces due to its excellent efficiency. Ball screw operation often occurs at 90% or higher. As a result of the electromechanical ball screw and bearing structure, friction is produced. The tracking accuracy declines as a result of dead zones and frictional forces. The number of system cycles and tracking performance can be limited by uncontrollable causes the system is still mechanical even though the friction force is regulated via a feedback controller. Resonance has an effect on the control loop's overall bandwidth. Other than mechanical Lead screw characteristics also had an impact on the system's overall performance. For example, location, speed, and confusion are all constrained by the brittleness of lead. The system's inertia is based on the first frequency that is natural. Cut back on the system control consumption. Eventually, this will result in shearing.

2.3 Performance Measure of Machines

Technology and techniques used in controlling precisely the movements of mechanical systems (such as robots, unmanned aerial vehicles (UAV), CNC machines) is known as motion control. A CNC machine is a sophisticated motion control related mechatronic system which consist of motors, feed drives, amplifiers, position-velocity-acceleration sensors, controllers and real time computer algorithms. The computer algorithm incorporated in the machine generate time based position commands via trajectory generation and close the axis servo loops. In motion control the demand for accuracy and precision can be achieved by using two major types of control algorithms; point-to-point (PTP) or positioning control and continuous path (CP) control or contouring control.

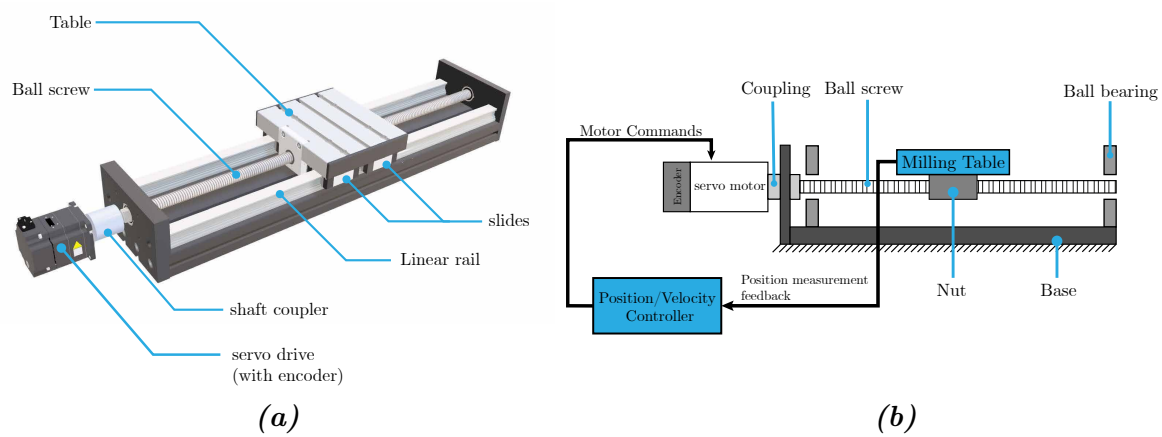

Figure 2.3: *Electromechanical Ball screw drive system; (a) Ball screw motor stage and (b) Structure of ball screw system*

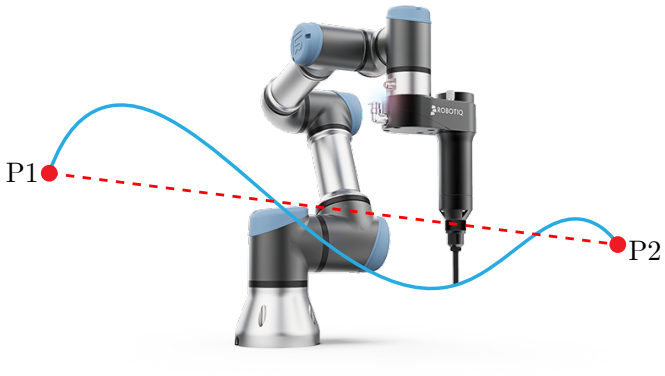

Figure 2.4: *point to point motion control*

i. point-to-point (PTP) control is the movement of points from one specific point to a another. The speed and acceleration of this control is usually optimized to product fast and accurate movements. However this movement is independent on the trajectory. This implies that the final end point is most important and the path taken by the object does not really matter; whether it moves from a straight, and arc or whatever direction. Example of this application can be found in pick and place applications, assembly lines, hydraulic presses or medical devices. As shown in Figure 2.4, the Universal Robot has to move from a starting pose P1, to final pose P2. Here, the trajectory taken by the robot is independent.

ii. Contour control on the other hand is the movement of an object through a series of defined points along a prescribed path. The speed and acceleration

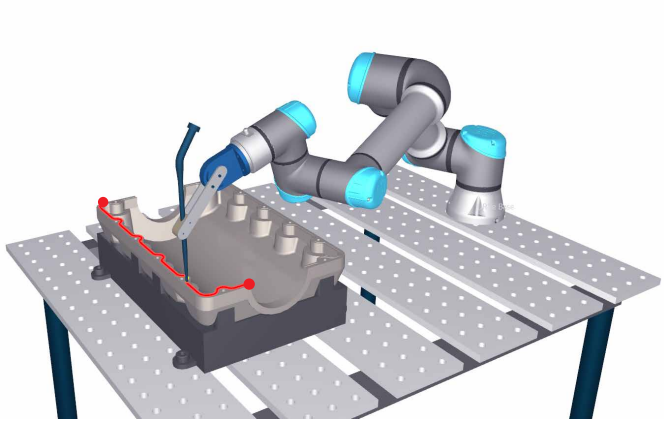

Figure 2.5: *Continuous motion control*

of the movements here can vary continuously along the trajectory and all points must be continuously monitored at each time interval up till the final end point. This control algorithm is used in application where the path taken by the machine is of concern. Example include; CNC machines, 3D laser cutting etc. As shown in Figure 2.5, The robot is dispensing glue on a specified trajectory. Fail in the trajectory will cause in ineffective bonding of the pieces to be glued. Thus contour control is important for this situation where the state of the robot is significant at successive time steps.

The properties of milling machines usually have performance characterisation including stability, robustness, disturbance depletion and transient responds. The performance characteristics of the drive system can be measured in the;- (i) time domain (ii) frequency domain.

2.3.1 Performance measure in time domain

By using a step response as input, the performance of the system can be evaluated in time domain. By visualising a plot of a step response as shown in Figure 2.6, the following characteristics can be noticed [Nise, 2019] [Sigurd Skogestad, 2005].

- *Rise time* (t_r): it is the time required for the output to reach 90% of its final value.
- *Settling time* (t_s): the time after which the output stays within ±5% of its final value.
- *Peak time* (t_p): the time required for the output to reach its maximum value.

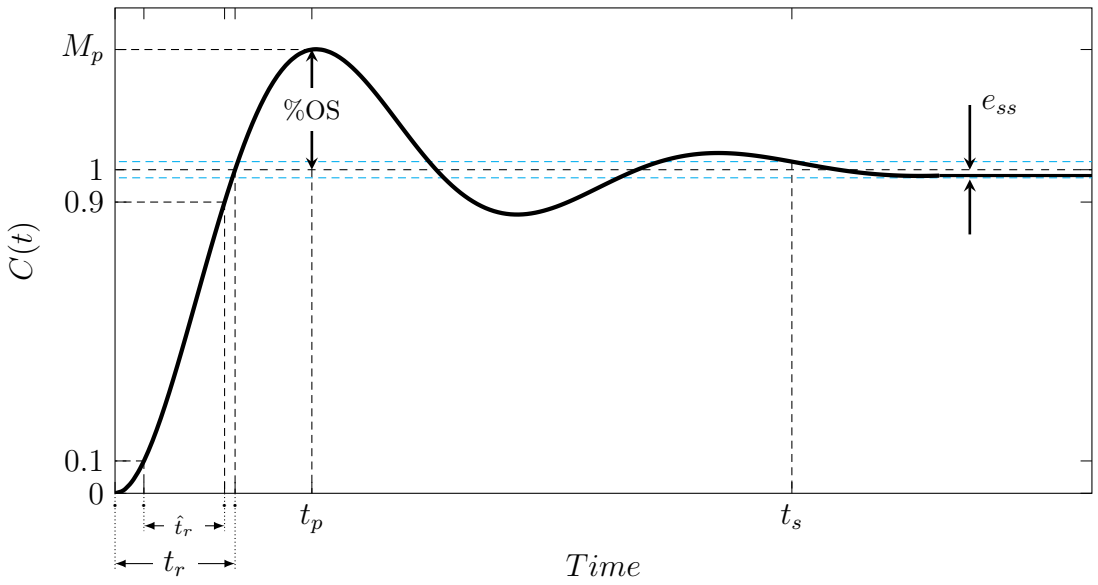

Figure 2.6: *Transient step response of a second order system.*

- *Overshoot*$(\%OS)$: the amount by which the output signal exceeds its final value, expressed as percentage of the steady state error.
- *Steady-state error*(e_{ss}): the difference between input and final desired output when the when the natural response has decayed to a value of zero.

2.3.2 Performance measure in frequency domain

Frequency domain, on the other hand just like time domain evaluates the performance of a system. one advantage of frequency domain over step responds analysis is that, it covers a wide range of signal classes (sinusoids of any frequency). This makes it easier to identify systems behaviour in its bandwidth (crossover) [Sigurd Skogestad, 2005].

In frequency responds, the basic facts governing design for stability, transient response, and steady-state error [Nise, 2019] respectively are;- Firstly, the Nyquist criterion tells us the stability of the system. An open-loop stable system is stable in close loop if the frequency response has a gain margin (GM) of less than 0 dB where the phase is 180°. Secondly, the percentage overshoot is reduces with increase in phase margin (PM), the increase in bandwidth leads to an increase in the speed of the responds. Lastly, increasing the low-frequency magnitude response improves the steady-state error. Skogestad et al. [Sigurd Skogestad, 2005] requires a heuristic value of $GM > 2$ and $PM > 30°$.

An important factor to consider when designing controllers of systems containing frequent uncertain disturbance is robustness. A robust controller is then defined as a the ability of that controller to resist and compensate variations, errors, and external disturbances while the performance of the system is unchanged.

2.4 Disturbance Forces in Machine Tools

As the demand for accuracy and precision increases in manufacturing industries, a significant amount of investigation has to be carried out on the disturbance forces that arises into machine tools. As these disturbance force arises from different sources, it is important for machine tool designers to design systems that will actively reject these disturbances during machine tool operation in order to achieve better tracking performance.

2.4.1 Mechanical Resonance

When designing dynamic system it is indeed important to consider its vibrating characteristics as this can lead to failure of the system. Resonance is a phenomenon where a system vibrates at its natural frequency. This signifies that the system is vibrating at it maximum frequency. In machine tools this also happens; thus, negatively affects the system and reduces the tracking performance of the machine tool. A common way to visualise resonance in machine tools is by using frequency responds function (FRF).

2.4.2 Mass vibration

The mass of the overall machine affects the system characteristics. when the mass changes, a significant concern should be taken into consideration as it decreases the accuracy and precision of the machine tool. Usually, when the total mass ratio of work piece to machine is so small, the total effect can be neglected. However, when the total mass ratio of work piece to machine is high, then some significant consideration should be taking to design an appropriate controller for these operational practices. This can be well explained with a mass spring damper system as shown in Figure 2.7. If the overall mass, M is changed considerably, a proper spring constant (K) and damping coefficient (b) should be chosen to achieve a desired specification due to an external applied force (F).

The building blocks of machine tools consist of mechanics, electronics and software. Mass variation in machine tools will lead to variation of inertia load to the linear axis module of the machine which is directly change the dynamics of these building blocks.

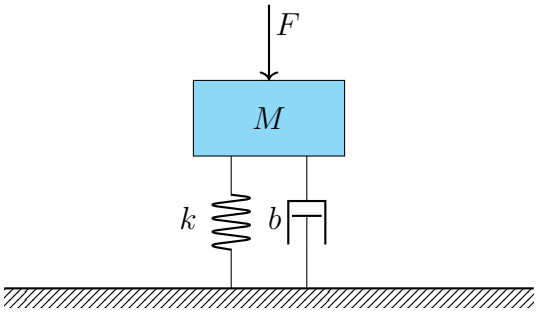

Figure 2.7: *Mass-Spring-Damper system*

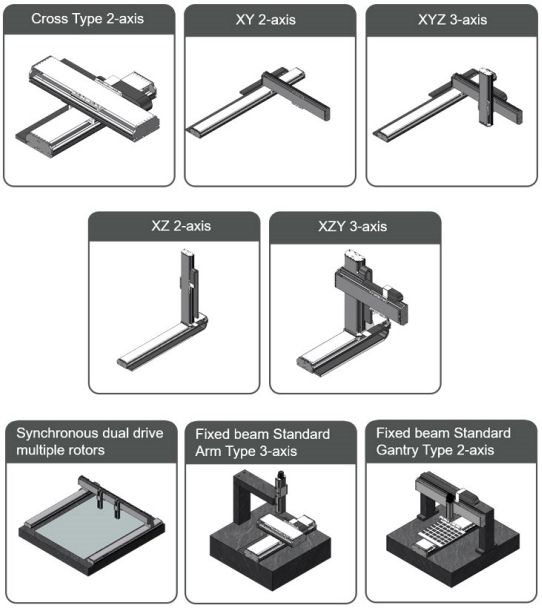

Figure 2.8: *Linear motor modules combinations, reproduced from www.kasite-linear-module.com*

A 3-axis CNC machines usually consist of X, Y, Z axis which are mounted into different configurations as shown in Figure 2.8. This combinations requires that a robust controller should be designed for the machine to function under a vast range of loads, otherwise there will be fluctuations in tracking performance leading to a undesired results during machining processes. As a result, a machine tool is said to be robust if it can operate under various weight of work pieces.

2.4.3 Friction Forces

Friction force is defined as a resistive force that opposes the relative motion of two bodies when they are in contact [Blau, 2008]. In machine tools, friction always exist which could cause wear and tear of the linear axis and also have a negative impact on the tracking accuracy of a machine tool. In some applications, machine tools friction guides. They used where speeds are generally below 0.5m/s. The properties of this include;- they have high good damping, strengths against load impact and high load capacity of 140 MPa, [Altintas et al., 2011]. The primary source of friction in mechanical drives develops between contact bearings of the drive motor and also between surfaces of the linear axis [Papageorgiou et al., 2020]. Friction in electromechanical systems is nonlinear. So, it is very essential to describe friction in systems where accuracy and precision is of major importance. In machine tools, friction force exist in three different natures [Maharof et al., 2020] [Blau, 2008];

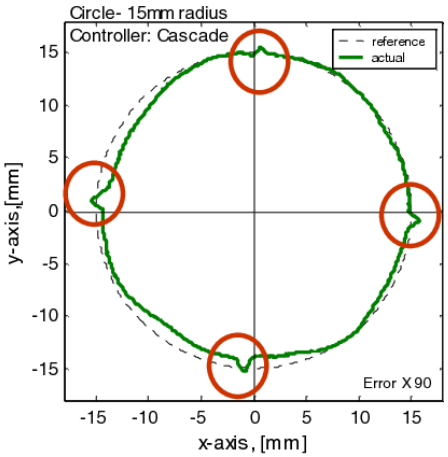

Figure 2.9: *Influence of quadrant glitches from a circular test [Jamaludin et al., 2008]*

(i) Friction Between the linear guide way and the bearing of the motors: this category is characterised by a property of contour tracking error called "spike". Spike refers to a sudden fluctuation which causes motion error in the linear drive system. This abnormally in circular interpolation routines[1] also arises at quadrant locations cause by the reversal of ball screw [Jamaludin et al., 2008]. This is named "Quadrant glitches". This can be illustrated as shown in Figure 2.9.

[1]circular interpolation is defined as motion along a circular path which is achieved by coordinating two machine axis simultaneously. This leave micron-level imperfections on the work piece

(ii) Friction Between the work piece and the cutting tool: This contact interaction helps the material to be sheared during the machining processes however, it also causes wear and tear of the machine tool causing the short life span of the cutting tool.

(iii) Friction which occurs between the table and guide ways.

The overall friction negatively affects the machining process by raising the overall power consumption of the machine tool.

2.4.4 Cutting Force

Machining in manufacturing is the removal of materials from the work piece by the use of a cutting tool in order to produce a desired shape. This cutting process at the end results in the production of chips[2]. The various cutting processes involved include;- Turning, Milling, Drilling and other conventional machining operations. The cutting tools is designed to have specific geometry and is usually stronger than the work piece. During material removal process, the main effect responsible for removing the material is shearing effect. shearing effect happens in the shear zone at an angle ϕ which is called Shear angle. Cutting tool contains an angle of relief called Rake angle, α which impacts on the chip disposal, tool performance and cutting force.

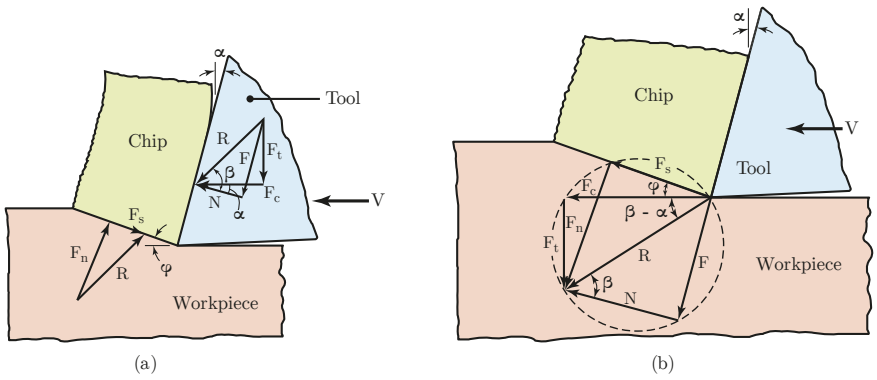

Figure 2.10: *(a) Forces acting in the cutting zone during two-dimensional cutting, where resultant force, R, must be colinear to balance the forces. (b) Force circle to determine various forces acting in the cutting zone. [Serope Kalpakjian, 2020].*

[2]Chips refers to the small pieces of materials that are cut out from the work piece during a machining process

Cutting force as related to CNC machines gives a negative effect on the tracking performance of the machine tool which reduces the accuracy and precision of the final machined part. With that said, it is important to characterise cutting force in machining. Consider a cutting force acting on a chip during orthogonal cutting process as shown in Figure 2.10. The cutting force, F_c acts in the direction of the cutting speed, V the trust force, F_t act in the direction normal to the cutting force. The combination of these two forces produces a resultant force, R. Furthermore, in the tool face, the resultant force is resolved into Friction force, F, and Normal force,N as shown in equation below.

$$F = Rcos\beta$$
$$N = Rsin\beta$$

Similarly, along the shear plane, the resultant force is also resolved into Shear force, F_s, and Normal force, F_n. It can be shown that these forces can be expressed as

$$F = F_c sin\alpha + F_t cos\alpha \tag{2.1a}$$
$$N = F_c cos\alpha - F_t sin\alpha \tag{2.1b}$$
$$F_s = F_c cos\phi - F_t sin\phi \tag{2.1c}$$
$$F_n = F_c sin\phi + F_t cos\phi \tag{2.1d}$$

The cutting forces F, N, F_s, and F_n from Equation (2.1), can not be measured directly during machine operation due to varying conditions of cutting conditions and tool geometries. Since the forces directions are known, force transducers like dynamo-meter can be aligned accordingly to measure them.

Friction forces also, deteriorates the machine tool and reduces tracking accuracy. As noticed, cutting force is important in machine tool operation as it produces the required force needed to shear materials from the work piece. Thus, milling parameters can also be involved in the negative effects of the cutting forces; depth of cut, feed rate, spindle speed also give information about the relation between milling parameters and cutting force. As stated by Kalpakjian et al. [Serope Kalpakjian, 2020] the cutting speed is expressed as;

$$V = \pi DN \tag{2.2}$$

where:

V = cutting speed (mm/min),

π = pi (radian),
D = diameter of cutter (mm),
N = spindle rotational speed (rpm)

As shown in Equation (2.2), the cutting speed is directly proportional to the spindle rotational speed and the diameter of the cutter. The feed, f in milling at constant diameter is described as feed per cutter, which represents the chip size generate at successive cutting edge. It can be calculated as,

$$f = \frac{V}{N \cdot n} \tag{2.3}$$

where:

f = feed per tooth (mm/tooth),
V = feed rate (mm/min),
n = number of teeth on the cutter,
N = spindle rotational speed (rpm)

As shown in Equation (2.2) and (2.3), the parameters are verified to be interrelated to each other. Changing one parameter will definitely affect the other, consequently, considering both Equation (2.2) and (2.3) is significant when choosing parameters of a milling operation.

2.5 Cutting Force Measurement Techniques

Cutting force data offers important insights into a variety of topics, including optimization, tool condition monitoring, and machining processes. For this reason, numerous scholars have utilized and explored a variety of techniques for measuring the cutting force. That section goes over and provides additional explanations for the four theoretically supported ways to measure info on cutting force which are Known by the following four names: capacitive displacement sensor; measuring the motor's current and the electromagnetic bearing's voltage, Current-sensor based, as well as dynamometer.

2.5.1 Capacitive displacement sensor

Capacitive displacement sensor technique was the first proven method [Albrecht et al., 2005] to compute the cutting force, which falls under spindle integrated sensor system. As illustrated in Figure 2.11, the capactive sensor S1, S2, S3 and s4 are externally fixed and makes use of a spindle cylindrical flange as set goal for the sensor. As the capacitance is created between the gap between the flange and

the capacitive sensor, a relation is developed where the cutting force is directly proportional to the displacement of the cylindrical spindle flange. The voltage generated due to the displacement is fed into a data acquisition hardware where it is further processed (e.g Using low pass filter) to normalize the data, thus providing accurate force measurement.

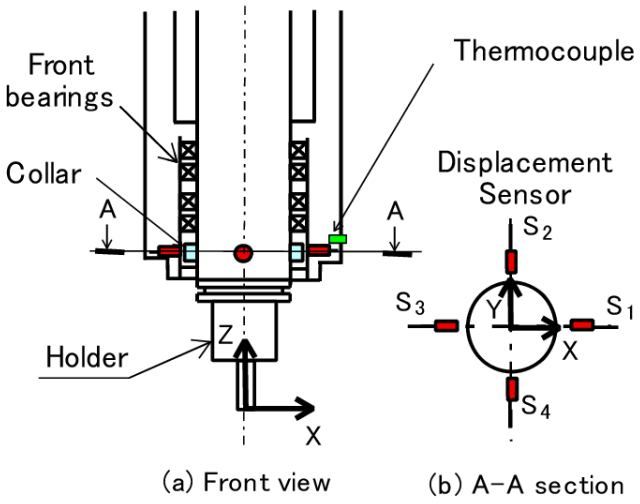

Figure 2.11: *Spindle-integrated capacitive displacement sensor configuration for determining cutting force [Sarhan et al., 2006]*

2.5.2 Current sensor based

The second method of measuring the cutting force is directly by the use of current probed in the servo drives used in the machine tool. As shown in Figure 2.12, the electric current makes used of dynamic lumped parameter model to classify the DC servo current in the CNC machine [Liang et al., 2016]. From the dynamic equation of a DC motor, the current present in the servo drives is directly proportional to the disturbance torque produced by the cutting force. This signifies that, when the cutting forces are large, the motor will require large amount of current to overcome the shear stress to remove materials on the workpiece forming chips. Thus, with a current sensor (placed after the drive motor) coupled with an acceleration sensor place to the tool bit, a large amount of data is collected and processed, where it is further passed through a prediction model in order to get the cutting forces.

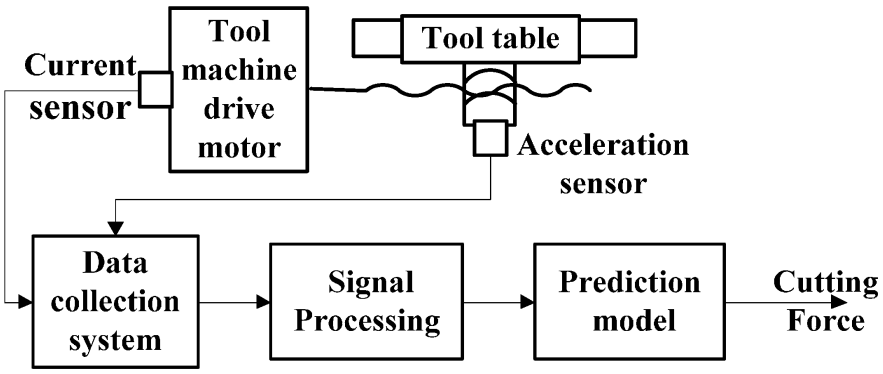

Figure 2.12: *Schematic diagram of current based cutting force sensing technique [Liang et al., 2016]*

2.5.3 Active Magnetic Bearings (AMB)

By taking advantage of the structure of electromechanical motors, another approach is proposed [Auchet et al., 2004] which utilizes an active electromagnetic bearings with magnetic levitation principles. Despite that, it eliminates problems including; bearing resistance, lubrication and mechanical wear. This method is accomplished by symmetrically placing electromagnets radially to the shaft, which exerts forces radially induced by the coil's current as shown in Figure 2.13. This provides an equilibrium position to the shaft. When there is a force that causes the shaft to deviate from equilibrium position, voltage commands are provided to the respective electromagnet causing them to produce forces in order to resettle the shaft to equilibrium position. The voltage commands is then collected to forecast cutting forces using regression techniques (like least square algorithm). Experimental results [Auchet et al., 2004] put in evidence a static accuracy and bandwidth of less than 8% at approximately 62 Hz, respectively, which was closely equivalent to a commercial Kistler measurement ecosystem.

2.5.4 Dynamometer

A Dynamometer is a device that measures force and torque. It is made up of piezoelectric materials that are stacked together between two plates. When force is subjected to piezoelectric materials, it generates a significant amount of charges which is converted to voltage. The voltage is measured by a processor, which determines the amount of force or torque applied. Figure 2.14, shows a Kistler FMD dynamometer which is used to measure the cutting force during a milling operation or turning process. The Kistler Dynamometer Type 9257B [Multicomponent Dynamometer, Kistler, nd] is specifically made up of three component

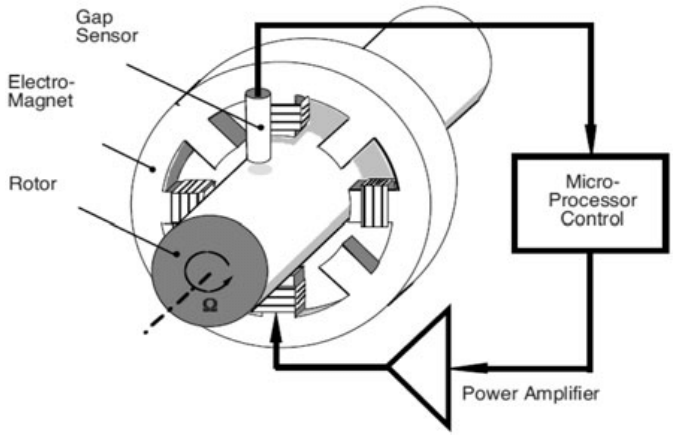

Figure 2.13: *Structure of active electromagnetic bearings [Saeed et al., 2013]*

forces built-in under high preload between two plates. Each force sensors have three pairs of quartz plates where two of them are shear responsive in the X-axis and Y-axis, and the other one to pressure responsive to the Z-axis. The mounting configuration is a "Sandwiched configuration" where the dynamometer is placed on the table and the workpiece is mounted on the dynamometer (using mounting points as in Appendix B). When force is applied to the dynamometer, the quartz materials generates charges measurement signal. The Kistler Dynamometer uses a multichannel charge amplifier to further amplify and convert the signal to readable signal data (electrical voltage), where the measured value is exactly proportional to the force.

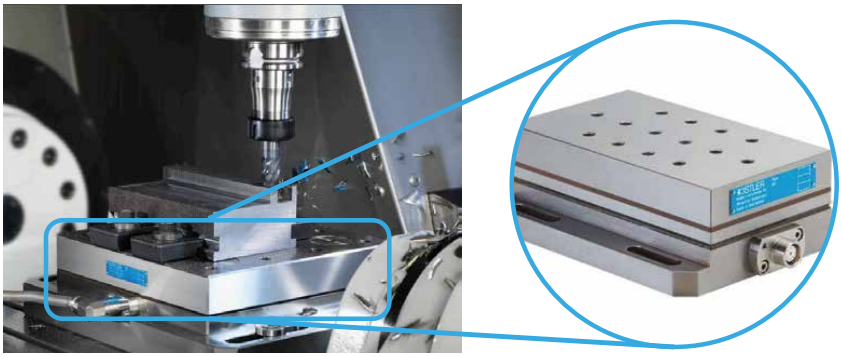

Figure 2.14: *Force measurement using Kistler Dynamometer*

In summary, four widely used methods exist for gathering cutting force data, according to the literature: dynamometers, active electromagnetic bearings, current-sensor-based systems, and capacitive displacement sensors. In essence, selection

criteria are based on precise and accurate measurement, equipment accessibility, financial resources, and literature-based advice. It is selected to use the Kistler Dynamometer model 9257B for the stated purpose since dynamometers are the most widely recognized tool for measuring cutting force data. Additionally, the equipment is easily accessible. The following stage is to analyze the cutting force data characteristics after the cutting force data has been successfully collected. In-depth discussion of these stages is provided in Section 3.5. The next section discusses different control solutions to counteract the influence of disturbance force on machine tool precision placement.

2.6 Controller design compensation strategies

In motion control, it is less often to redesign the hardware (mechanical and electrical subsystems which is costly) in order to produce extremely accurate precised machining. With that said, once the machine tool is built, the only flexibility left is to design a proper control technique which will successfully compensate uncertainties, attenuate for noise and reject disturbance forces. In regards to compensation strategies, many control approaches have been used which are classified into, classical control, advanced control and model-based control techniques. These approaches aim to improve the performance, but their characteristics depends on their nature.

2.6.1 Classical control techniques

Classical control is a branch of control theory commonly applied in industry by using basic tools to describe and model the system. Examples of classical control techniques is PID control; This is one of the most used control technique in the field of control systems. A great academic and industrial lay their basis on this technique which is relatively simple, effective and easy to tune. PID is a benchmark for closed loop controllers and the analytical approach of designing a PID control is relatively simple without the need of deep knowledge of control theory. Additionally, another control law common in motion control is cascaded P position and PI velocity control. Last but not least Lead-lag control is also one building block classical control theory that improves undesirable frequency responds in closed loop systems.

2.6.2 PID controller

PID controller provides an efficient and simplest way solution to real world control problems in the industry. With the advent of digital tools, a lot of industries

still use PID algorithms due to its applicability, simplicity and transparent functionality. A PID controller might be considered as a lead lag compensator with one pole at origin and another one at infinity. A PID controller is also termed as "Three-term" controller written in "parallel form" as in Equation (2.4). It consist of three terms; Proportional (P), Integral (I) and Derivative (D). The block diagram in Figure 2.15, illustrates the structure of a PID controller and how these three terms are applied.

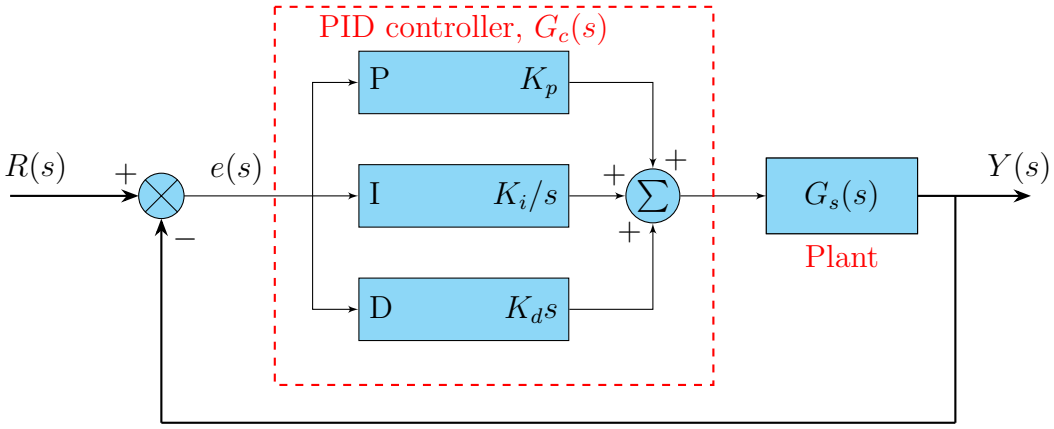

Figure 2.15: *Basic block diagram layout of a PID controller with feedback loop*

$$G_{PID}(s) = K_p + \frac{K_i}{s} + K_d s \tag{2.4}$$

where the terms K_p, K_i, K_d are the gains of the P, I and D controllers respectively. The PID controller have the following functionalities; - The proportional controller (P)–Provides an overall control action proportional to the error signal. - The Integral controller (I)–Reduces the steady-state error through low frequency compensation - The derivative controller (D)–improve the transient responds of the system through high frequency compensation.

- The proportional controller (P) – Provides an overall control action proportional to the error signal.
- The Integral controller (I) – Reduces the steady-state error through low frequency compensation
- The derivative controller (D) – improve the transient responds of the system through high frequency compensation.

The P, I and D controllers independently can have distinct effects on the performance of a closed loop system. This is achieved by changing the values of the gains K_p, K_i, K_d. Table 2.1, shows a summary of these individual effects based on performance index criteria.

Table 2.1: *Effects of individual controller gains K_p, K_i, K_d on closed loop system*

Closed-loop Response	**Rise time** (T_r)	**Overshoot** ($\%OS$)	**Settling time** (T_s)	**Steady-state error** (e_{ss})
K_p	Decrease	Increase	Small increase	Decrease
K_i	Decrease	Increase	Increase	Large Decrease
K_d	Small decrease	Decrease	Decrease	Small change

Controller parameters are often tuned in order for the closed loop system to be stable and meet some properties;- stability robustness, elimination of noise and robustness with respect to environmental and plant uncertainties, performance at transient (incorporating rise time, overshoot and settling time). More so, variations of PID tuning methods [Ang et al., 2005] have been demonstrated in literature which include;-

- Analytical methods; Where the model must be accurate and use algebraic relations between the plant and objective.

- Heuristic methods; This involve manual experimental tuning (for example Ziegler – Nichols method) and artificial intelligence (Fuzzy logic and Neural networks)

- Frequency responds methods; Its a fundamental method Where stability robustness if the highly desired characteristics of the system (Example include loop shaping)

- Optimization methods; Genetic Algorithm (GA).

- Adaptive methods; Include auto tuning algorithms on real time identification.

Loop shaping control design approach is a fundamental approach in designing PID controllers where the gain parameters are selected for the open loop system to have particular performance characteristics of the closed loop system. Analysis of the index performance criterion is mostly targeted to optimize the system dynamics and suppress the tracking errors. Figure 2.16, shows a feedback control system where we have the reference input, output and error signals represented by $r(t)$,

$y(t)$ and $e(t)$ respectively. Additionally, K_t, $d(t)$ and $n(t)$ represent motor constant, external disturbance and noise of the feedback sensor respectively. On the other hand, $G_p(t)$ and $G_c(t)$ represent the plant and controller respectively.

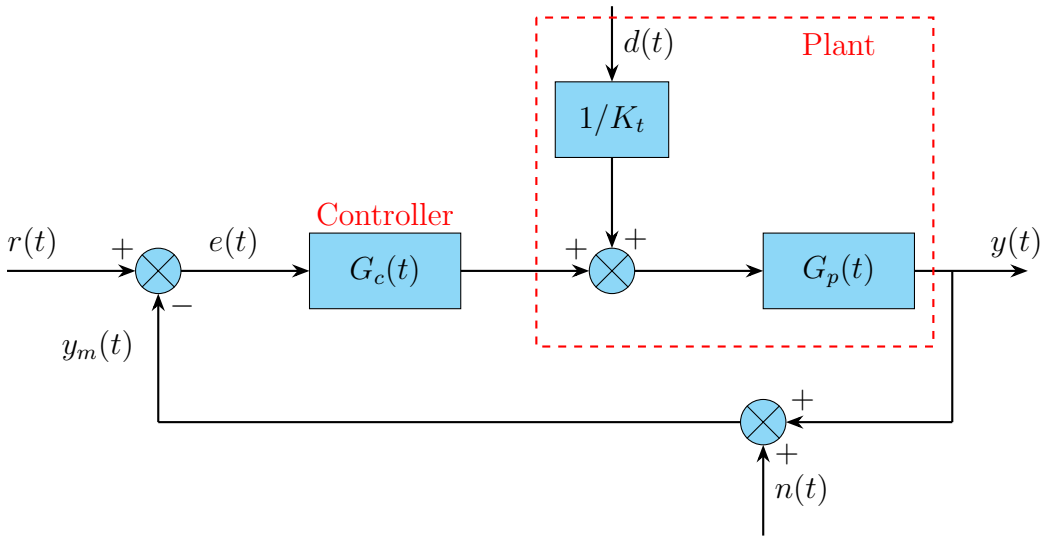

Figure 2.16: *Basic block diagram of a feedback system with PID controller with external disturbance*

The input to the controller $G_c(s)$ is $E(s) = R(s) - Y_m(s)$, where $Y_m(s) = Y(s) + N(s)$. Thus the error signal term in frequency domain can be expressed as shown in equation (2.5).

$$E(s) = R(s) - Y(s) - N(s) \tag{2.5}$$

The plant model is written as

$$Y(s) = \left[G_c(s) \cdot E(s) + \frac{D(s)}{Kt}\right] \cdot G_p(s) \tag{2.6}$$

Substituting Equation (2.5) in (2.6), we obtain (2.7) which is the system output $y(t)$ represented in the frequency domain.

$$Y(s) = \frac{G_c(s) \cdot G_p(s)}{1 + G_c(s) \cdot G_p(s)} R(s) + \frac{G_c(s)}{[1 + G_c(s) \cdot G_p(s)] \cdot K_t} D(s) - \frac{G_c(s) \cdot G_p(s)}{1 + G_c(s) \cdot G_p(s)} N(s) \tag{2.7}$$

Combining Equation (2.5) and Equation (2.7), we obtain the control error which is further simplified in terms of $r(t)$, $d(t)$, $n(t)$ as shown in Equation (2.8).

$$E(s) = \frac{-1}{1 + G_c(s) \cdot G_p(s)} R(s) + \frac{G_c(s)}{[1 + G_c(s) \cdot G_p(s)] \cdot K_t} D(s) - \frac{G_c(s) \cdot G_p(s)}{1 + G_c(s) \cdot G_p(s)} N(s) \tag{2.8}$$

The following notations and terminologies are derived as illustrated from Equation (2.9) to (2.11). $L(s)$ represent the open loop transfer function which determines the gain margin (GM) and phase margin (PM). $T(s)$ represents the closed loop transfer function from reference signal to output signal. Lastly, $S(s)$ represents the sensitivity function which provides the bandwidth of the system due to the output disturbance.

$$L(s) = G_c(s) \cdot G_p(s) \tag{2.9}$$

$$T(s) = \frac{G_c(s) \cdot G_p(s)}{1 + G_c(s) \cdot G_p(s)} \tag{2.10}$$

$$S_{pid}(s) = \frac{1}{1 + G_c(s) \cdot G_p(s)} \tag{2.11}$$

The goal for stability is to design a stable controller that will compensate uncertainties, reject disturbances and attenuate noise. The target is to design $G_c(s)$ such that Equation (2.9) to (2.11) have specific desired properties. We Design $G_c(s)$ such that; the system has good reference tracking such that $Y(s) = R(s)$, disturbances are rejected so $S(s)$ is so small for frequencies that a range of frequencies are expected.

$$\zeta = \frac{-\ln(\%OS/100)}{\sqrt{\pi^2 + \ln^2(\%OS/100)}} \tag{2.12}$$

Equation (2.12) also illustrates the damping ratio, ζ, with respect to overshoot of the system [Nise, 2019]. In machining, more damping is required for better performances. The stability is established by using the Nyquist's plot with respect to the open loop transfer function; it ensures that at point $[-1, 0]$ is not encircled by the Nyquist plot [Sigurd Skogestad, 2005].

2.6.3 Cascade controller

Other than PID, cascade controller is another type of classical controller that is very used in the Industry. It makes use of multiple control loops that have multiple

signals to manipulate a single variable. This control technique enables the system to be more disturbance responsive. The basic form of cascade controller consist of two control loops using two measured signals to control a desired variable. In this work (related to machine tools), our cascade controller will consist of a position and velocity loop as shown on Figure 2.17, (where the position loop is build over the velocity loop)The velocity loop can be either a P or PI controller while the position is a P controller. For this control scheme we will use a PI controller. As stated in literature [Jamaludin et al., 2007a], this approach improves the performance of system containing disturbances.

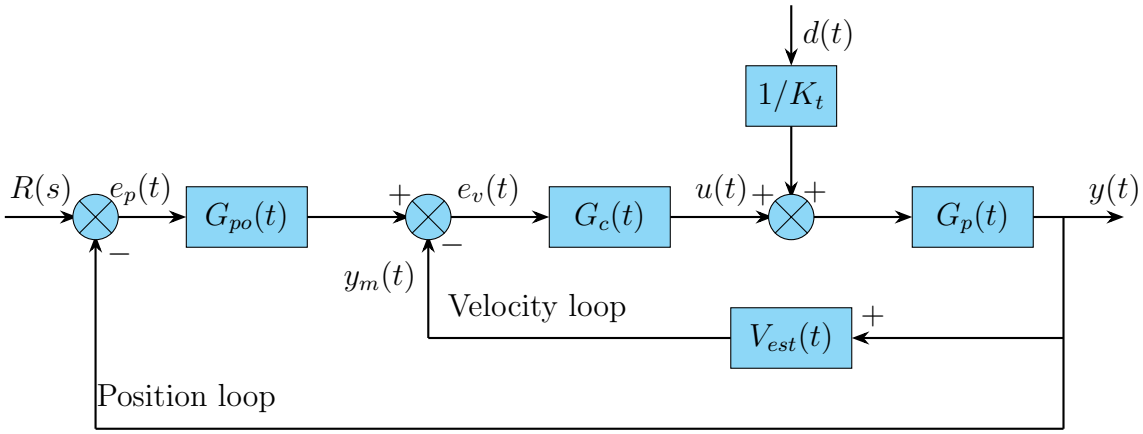

Figure 2.17: *Structure of a cascade P/PI controller*

The analysis of cascade controller is performed by first the velocity closed loop, followed by the position closed loop. Based on figure 2.17, the open loop, closed loop and sensitivity transfer functions of velocity loop of the controller are shown in Equation (2.13), (2.14) and (2.15) respectively.

$$L_{vel}(s) = G_{pi}(s) \cdot G_s(s) \tag{2.13}$$

$$T_{vel}(s) = \frac{G_{pi}(s) \cdot G_s(s) \cdot V_{est}(s)}{1 + G_{pi}(s) \cdot G_s(s) \cdot V_{est}(s)} \tag{2.14}$$

$$S_{vel}(s) = \frac{1}{1 + G_{pi}(s) \cdot G_s(s) \cdot V_{est}(s)} \tag{2.15}$$

Similarly, the open loop, closed loop and sensitivity transfer functions of position loop of the controller are shown in Equation (2.16), (2.17) and (2.18) respectively.

$$L_{pos}(s) = \frac{G_p(s) \cdot G_{pi}(s) \cdot G_s(s)}{1 + G_p(s) \cdot G_s(s) \cdot V_{est}(s)} \tag{2.16}$$

$$T_{pos}(s) = \frac{G_p(s) \cdot G_{pi}(s) \cdot G_s(s)}{1 + G_p(s) \cdot G_s(s) \cdot V_{est}(s) + G_p(s) \cdot G_{pi}(s) \cdot G_s(s)} \tag{2.17}$$

$$S_{pos}(s) = \frac{1}{1 + G_p(s) \cdot G_s(s) \cdot V_{est}(s) + G_p(s) \cdot G_{pi}(s) \cdot G_s(s)} \tag{2.18}$$

Again, the position steady-state error transfer function can be expressed as in Equation (2.19),

$$E_p(s) = A \cdot R(s) - B \cdot D(s) \tag{2.19}$$

where:

$$A = \frac{1 + G_{pi}(s) \cdot G_s(s) \cdot V_{est}(s)}{1 + G_{pi}(s) \cdot G_s(s) \cdot V_{est}(s) + G_p(s) \cdot G_{pi}(s) \cdot G_s(s)}$$

$$B = \frac{G_s(s)/K_t}{1 + G_{pi}(s) \cdot G_s(s) \cdot V_{est}(s) + G_p(s) \cdot G_{pi}(s) \cdot G_s(s)}$$

As cascade control consist of velocity and position control as shown above, it is highly used in machine tool applications due to its ability to reject disturbances. The cascade structure is makes its foundation on Proportional (P) and Proportional-Integral (PI). [Jamaludin et al., 2007a], performed a comparative study and observed that the performance of cascade control outweighs that of PID due to its structure; containing a velocity loop control which PID does not. However, cascade also have drawbacks when it comes to nonlinear systems. In order to implement cascade with nonlinear systems it is necessary to modify its control configurations as proposed by [Jamaludin et al., 2007a]. The technique uses a velocity and acceleration feedforward to reduce the tracking performance. The tracking performance of a cascade controller can be characterised based on its closed loop bandwidth, damping ratio and dynamic stiffness. Dynamic stiffness is defined as the inverse of the transfer function, which is an important parameter that determines how good a controller can reject disturbance.

2.7 Advanced Control Techniques

After analysing the literature of classical control, it is important to consider its limitations. In industry, advanced process control are usually stacked additionally onto basic controls. It usually involves complex analysis than classical control algorithms. Advance control is a high level control strategy that provides specific characteristics to low level loops to achieve an optimal desired performance. Every control law requires a process model. A Process models captures the behaviour

of the dynamic system relating the output behaviour due to a changed set point. This could be qualitative, mathematical and statistical.

Control systems can be also sometimes classified into two broad categories; Linear and nonlinear control systems. Linear control systems are those where the input varies linearly with the output. This is well defined mathematically where the input scales the output by a constant (they obey the principle of superposition). Examples of Linear control techniques include; PID, cascade and Linear Quadratic Regulator (LQR). On the other hand, nonlinear systems are those where the output signal varies nonlinearly with respect to the input (which does not obey superposition principle). These makes them more challenging and complex to analyze. Nonlinear control gives the best response and performance to a system and might also be implemented into linear systems when the demand of performance and accuracy is extreme. A simple nonlinear controller include Nonlinear Cascade Feed Forward (NCasFF) and Nonlinear PID (N-PID) which are changed applied to cascade and PID controllers respectively. Moreover, other examples of nonlinear controllers popular for their robustness, disturbance rejection and uncertainty compensation include Gain Scheduling (GS) controller, Sliding Mode controller (SMC) and H-infinity (H_∞)

2.7.1 Sliding Mode Control (SMC)

Sliding Mode control falls under the category of an advanced control. It is popular for its robustness features and fast dynamic responds with respect to high order nonlinear systems operating under uncertainty conditions. In control theory, uncertainties can be classified as Structured (or parametric) and Unstructured (unmodeled dynamics) uncertainties. Structured uncertainties can be due to the inaccuracies which are produced by the model itself while unstructured uncertainties addresses inaccuracies in the system order [citeeee]. Sliding methodology is based on the fact that 1st order systems are simple to control. This approach is implies simplifying an nth order system into a first order which leads us to a modified control law with a promising trade-off between tracking error and uncertainties. SMC algorithm initially introduced by [Utkin, 1977] which was impressive in its applicability in real time systems and characterized by its non linearity.

The development of SMC controller starts with Single-Input Single-output (SISO) which helps develop a strong intuition. Consider a second order system with SISO,

$$\ddot{x} = f(x) + g(x) \cdot u \tag{2.20}$$

$$y = x \tag{2.21}$$

where, $u(t)$ is the control input, $y(t)$ is the control output and $x(t) = \left[x, \dot{x}, \ldots, x^{(n-1)}\right]^T$ is the state variable, . Also $f(x)$ and $g(x)$ are nonlinear and are not known. The limited unknown functions are defined as $f(x) \leq f_0$ and $g(x) \leq g_0$. The error is defined such that;

$$e(t) = y(t) - y_d(t) \tag{2.22}$$

where, y_d is the desired reference input. The target is to achieve a tracking task such that $e(t) = 0$ which implies that

$$y(t) = y_d(t)$$

SMC methodology involves two criteria; namely, the feedback control law, u and the sliding surface.

2.7.2 Sliding Surface

The first step in designing SMC requires the design of a custom sliding manifold. The sliding function $S = f(e, \dot{e}, \ddot{e}, \ldots, e^{(n-1)})$ Furthermore a general formula representing a time varying surface is denoted by

$$S(t) = \left(\frac{d}{dt} + \lambda\right)^{n-1} \cdot e(t) \tag{2.23}$$

where n is the relative degree of the system and λ is a positive constant, $\lambda \in \mathbb{R}$ and is called the gain of sliding function. This illustrates that the order of the system has reduced from $x^{(n)}$ to S. The function S therefore is independent on the parameter of the system but only a function of a constant gain, λ and error, $e(t)$; which illustrates the robustness of the control algorithm. For example; for first order $n = 1$, $S = e$, for second order $n = 2$, $S = \dot{e} + \lambda e$.

2.7.3 Designing the control law

After defining the sliding surface, we define the sliding function such that $S = 0$ and $\dot{S} = 0$. The target is to shift all the variables into the sliding manifold and turn them to zero by designing a relay control. A conventional relay function is denoted by a signum function. Thus, the discontinuous control input is denoted by;

$$u_s = u_0 \cdot \mathrm{sgn}(S) = \begin{cases} -u_0 & \text{if } S < 0 \\ 0 & \text{if } S = 0 \\ u_0 & \text{if } S > 0 \end{cases} \tag{2.24}$$

A general a graphical representation of SMC control strategy using a phase-plane, where $e(t)$ and $\dot{e(t)}$ represent axis is illustrated in Figure 2.18, Applying $u_s(t)$ to the system results in the movement of initial states to anywhere in the plane of the sliding function; this is termed as reaching phase. Furthermore it then slides along the surface to a desired target; this is known as sliding phase.

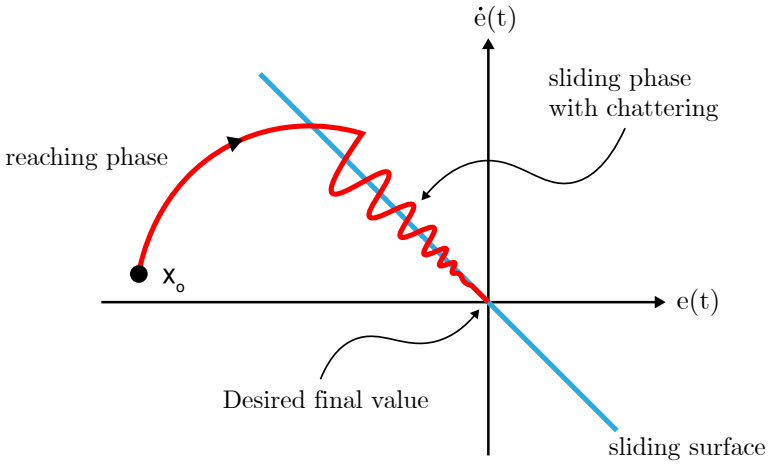

Figure 2.18: *Graphical representation of SMC*

Filippov's construction [Christopher Edwards, 1998b] provides an equivalent dynamic control input for SMC. The goal of the control law is to ensure that all the controlled variables are forced to its reference value, i.e, the state $e(t)$ and its derivative $\dot{e(t)}$ must be equals to zero. This is accomplished through,

$$\frac{dS(t)}{dt} = \dot{S}(t) = u_{eq} = 0, \tag{2.25}$$

where $u_{eq}(t)$ represents a continuous control input. The control input $u(t)$ finally consist of two additive parts; a continuous portion, $u_{eq}(t)$, and a discontinuous portion, $u_s(t)$. The resulting control input is denoted as shown in equation (2.26)

$$u(t) = u_s(t) + u_{eq}(t) \tag{2.26}$$

Adding the control input $u_{eq}(t)$ to $u_s(t)$ results in the decrease in reaching phase time delay.

2.8 Research gap

The final aim of this bachelor thesis is to design a robust stable control system of a ball screw CNC machine tool which will compensate for uncertainties, attenuate noise and reject disturbances that are generated during milling cutting process. This control system is accomplished in order to meet the demand for accuracy and precision. Despite the fact that, precise control scheme can be applied to machine tool to meet these demands, cutting and disturbance forces can not fully be avoided or eliminated. Various techniques have been proposed in literature which could be either ranging from classical methods to more complicated or advanced methods.

The control technique we propose in the thesis consist of a simple but yet, standard and popular PID contoller, cascade P/PI position controller and Sliding Mode Controller (SMC) to compensate for the high magnitude disturbance force in a ball screw XYZ position milling table. The control schemes is not only limited to machine tool but could be applicable to other mechatronics systems like manipulators joints control. Table 2.2 shows a summarized analysis on the different controllers based on their strengths and weaknesses.

Table 2.2: *Summary of literature reviews on control techniques*

Control technique	**Strength**	**Weakness**
PID	• Simple to design • Easy to tune • Only comprises of position loop	• Vulnerable to disturbance • Weak in performance
Cascade P/PI	• Easy to tune • Consist of both velocity and position control loop • Relatively easy in application	• limited to controlling nonlinear and higher order systems
Sliding Mode Control (SMC)	• Robustness • Good disturbance rejection properties • Applicable for nonlinear and higher order system (super twisted sliding mode)	• Chattering effect in control input which causes reduction in life span of motors

Comparing the approaches as stated, Cascade P/PI controller provides more advantages over PID controller in systems which demands precision and disturbance rejection. Cascade thus is perfect for machine for this application due to its configuration consisting of position and velocity loops. However, PID only consist of position control only thus has a limitation when it comes to velocity control. In terms of a more advance control which is SMC, provides a better robustness compare to PID and Cascade P/PI due to its ability to maintain tracking errors and reject disturbances at different spindle frequencies. Additionally, due to mathematical structure of SMC, it is able to compensate for the unmodeled dynamics of the with respect to the cutting force. Figure 2.19, illustrates an overall summary of the conducted litterature review.

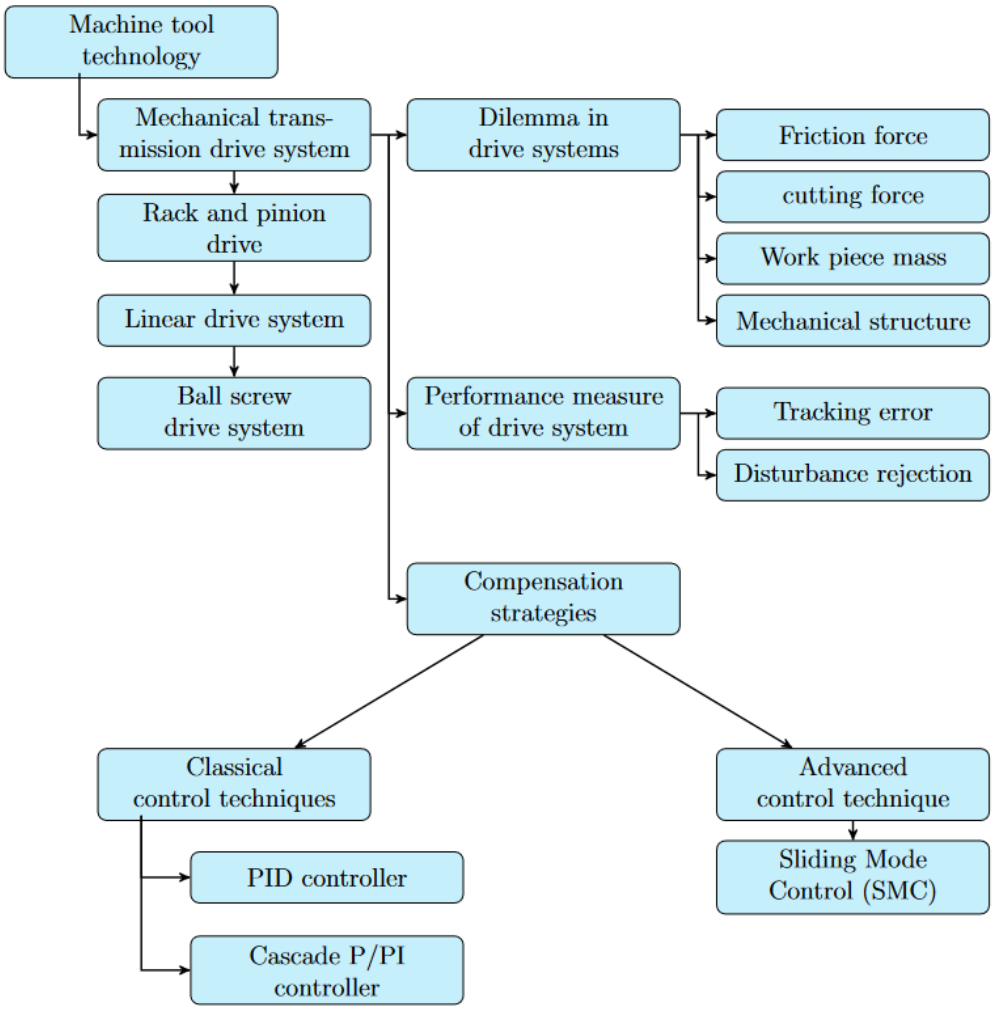

Figure 2.19: *Overall overview of literature review*

Chapter 3

METHODOLOGY

3.1 Introduction

In this chapter, the methodology is introduced the steps to carry out the design. The goal is to design an effective controller which will compensate for the cutting forces disturbance and thus improve the tracking performance. With the description of the previous control techniques reviewed in the previous section, this thesis applies this techniques accordingly.thesis.

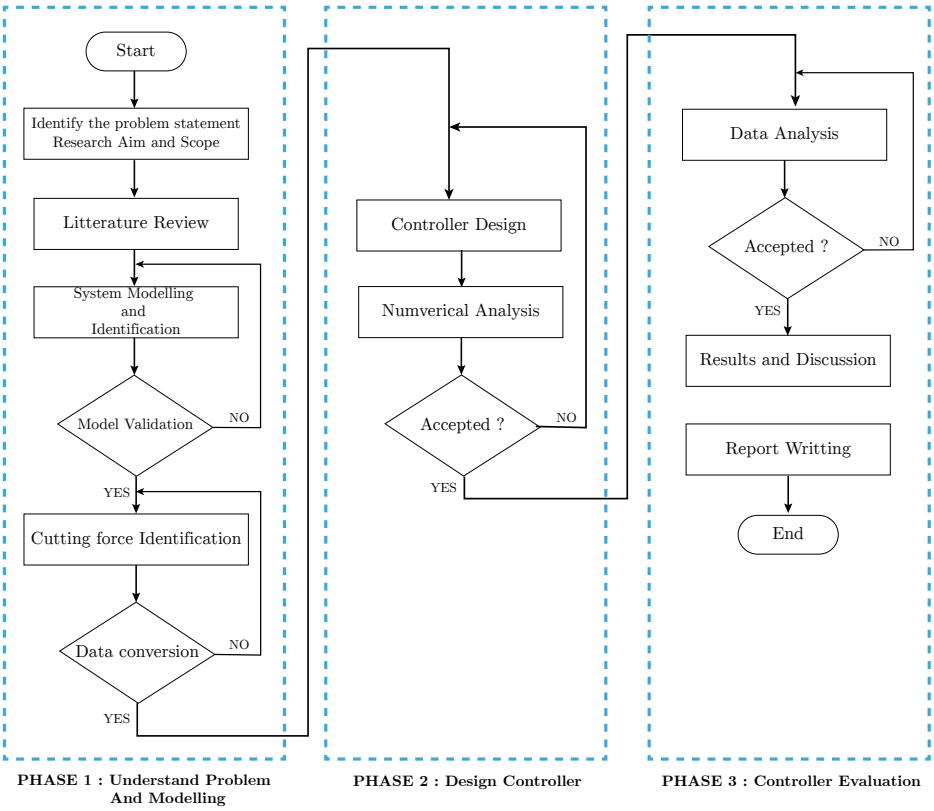

Figure 3.1: *Flow chart of research Methodology*

The Frequency Response Function (FRF) is used to specify the transfer function through system identification. Simultaneously, the cutting forces are analysed in the frequency which determines the harmonics frequencies in regard to the spindle speeds. This measured cutting force is then input to the system as an external

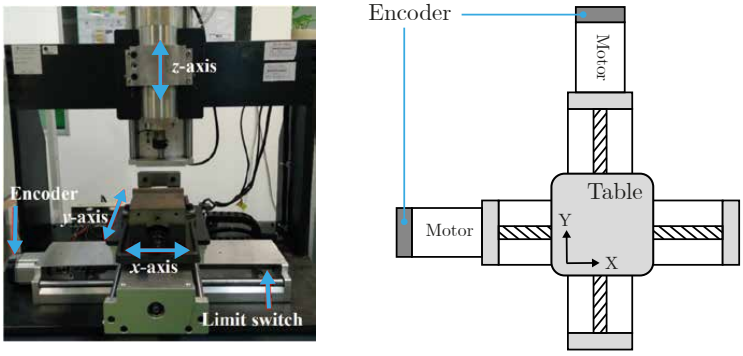

(a) (b)

Figure 3.2: *(a) ball screw driven XY positioning milling table system by Googol Tech (b) 2D diagram of X and Y axis milling table*

disturbance. Furthermore, the next step involves the design of the classical techniques; PID controller and P/PI cascade. Followed by the advanced technique; Sliding Mode Control (SMC). The control performance are further compared by performing the maximum tracking error, Root Mean Square Error (RMSE) and Fast Fourier Transform (TFT). Figure 3.1, illustrates the overall flow chart of the

3.2 Experimental Setup

The overall system considered in this thesis is a XYZ configuration positioning system from Googol Tech as shown in Figure 3.2(a) and (b). The milling machine consist of Panasonic MSMD 022GIU servo drives which moves every axis. Here, system identification is performed only on the X axis. Thus, X axis is considered in order to reduce the coupled dynamics of the other axis of the machine. The instance of a Z axis is also not considered as the proceeding work only considers only a fix depth of cut. As illustrated in Figure 3.2(a), the spindle is attached on the Z axis, X axis represents the motion horizontal direction and Y axis is the motion in the vertical direction when viewed from top. The dimension of the XY positioning milling table is $600 \times 470 \times 815$ mm, length, width and height respectively. The incremental encodes equipped by the X and Y axis provides a resolution of 0.0005 mm/pulse. Added to that, the axis is provided with limit switches for homing and safety measures. Further specifications of the machine is provided in Appendix A.

The overall system configuration is made up of the following a personal com-

puter with MATLAB/Simulink[1] and ControlDesk [2] software as shown in Figure 3.3, ControlDesk software also integrates a digital signal processing (DSP) board, dSPACE DS1104. The DSP board linked with the servo amplifier serves as a digital Input/Output interface for the system; provides data acquisition platform and signal output to the plant. The servo drive converts the digital inputs from the DSP board to analog in order to drive the motors. Simultaneously, the DSP board also provide enable/disable commands to the plant and homing sequence. The amplifier augments the actuator signals by a factor of ten. The section that follows describes the modelling and system identification procedures of the plant.

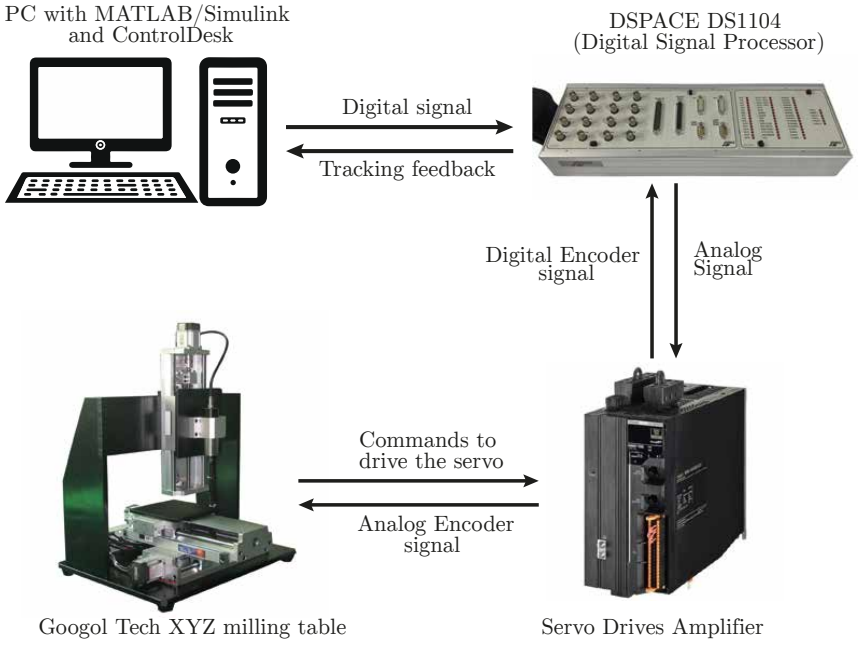

Figure 3.3: *Experimental setup overall system configuration*

3.3 System Modelling and Identification

System identification is one of the widely used process to determine the mathematical model of the dynamic system relating the input and output. This thesis referenced a frequency domain identification due to data and noise reduction. The system dynamics was represented as a Single-input Single-output (SISO) model,

[1]MATLAB/Simulink. www.mathworks.com/products/simulink.html

[2]ControlDesk.www.dspace.com/en/inc/home/products/sw/experimentandvisualization/controldesk.cfm

which was determined from the Frequency Response Function (FRF) of the system from input voltage to encoder position signals [Maharof et al., 2020]. After data collection and analysis, the process yield a second order function with time delay which is stated by Equation (3.1). Where $Y(s)$ is the position output (mm) and $U(s)$ is the input voltage (V). Table 3.1, list the constants A, B, C and time delay, T_d of the system.

$$G_m(s) = \frac{Y(s)}{U(s)} = \frac{A}{s^2 + Bs + C} e^{-s \cdot T_d} \tag{3.1}$$

Table 3.1: *Parameters of system model*

Parameter Constant	A (mm/V· s^2)	B (s^{-1})	C (s^{-2})	T_d (s)
Value	78020	163	193.3	0.0012

3.4 Identification of motor constant

During milling operation, It is important convert the disturbance forces (cutting and friction forces) to voltage. This is achieved by a motor constant K_t, used throughout the design process. A mass model as referred from [Maharof et al., 2020] is used as shown in Figure 3.4. K_t in Newton per Volt (N/V) relates the Force, F, in Newton (N), and input voltage to the motor drives, u, in Volts (V). M represents the unit mass of the system in Kilograms (kg) and v is the velocity in meters per second (m/s). Equation (3.2), compares the simplified model equation with equation derived from open loop system which when simplified results in Equation (3.3). Where M is the Mass of the system in Kilograms (kg) and $\bar{G}$ is equivalent to parameter A as from Equation (3.1) in mm/V·s^2. Thus, the x-axis positioning motor constant, K_t was calculated, resulting in 2871.14 N/V.

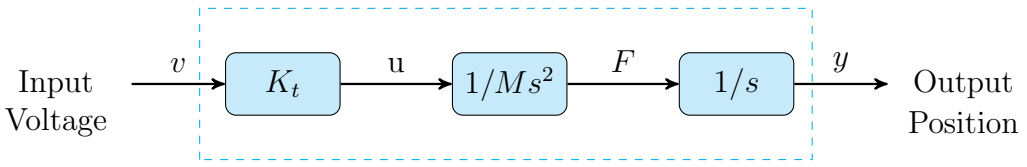

Figure 3.4: *Block diagram of the open loop system for motor constant identification and force estimation (Jamaludin, 2008)*

$$\frac{Y(s)}{U(s)} = \frac{\bar{G}}{s^2} = \frac{K_t}{Ms^2} \tag{3.2}$$

$$K_t = \bar{G} \cdot M \tag{3.3}$$

3.5 Cutting force measurement and quantification

In the development and design of an accurate and precise controller, cutting force measurement and analysis is the benchmark. A sequence of cutting forces are carried out using different parameters, which is further applied as disturbance input during numerical validation of the controller. As suggested by [Serope Kalpakjian, 2020], the typical interval of both feet per tooth and depth of cut are 0.1-0.5 mm and 1.0-8.0 mm respectively. This parameters produced three distinct data for spindle speeds. The feed rates performed were 1200 mm/min, 2000 mm/min and 2800 mm/min for spindle speeds of 1500 rpm, 2500 rpm, 3000 rpm respectively. This parameters provided a framework as follows; the initial stage involved establishing the cutting force measurement, followed by designing experiments to characterize cutting forces in the second phase, and concluding with the analysis and characterization of these cutting forces in the final phase.

3.5.1 Cutting force measurement experimental setup

During the conduction of the milling cutting process, a conventional milling machine was used and various equipment where simultaneously used to measure the cutting forces. These equipment is shown in Table 3.2. The system diagram used in measuring the cutting forces is shown in Figure 3.5, A straight-line milling cutting operation was performed on the Aluminium block using HSS (10 mm Dia., 4 flute cutter edges) with different the passes of spindle speed 1500 rpm, 2500 rpm and 3000 rpm. Using the Kistler 9257B Dynamometer mounted on the milling table using four Allen cap screws M8×50mm, the cutting force was obtained.

Table 3.2: *Equipment List with specification*

List of equipment	**Description**
Model of milling machine	Gate PBM VS 400
Cutting tool material	High Speed Steel (HSS)
Cutter diameter	10 mm
Cutter's edges number	4
Workpiece material	Aluminium (Al)
Dynamometer's model	Kistler 9257B

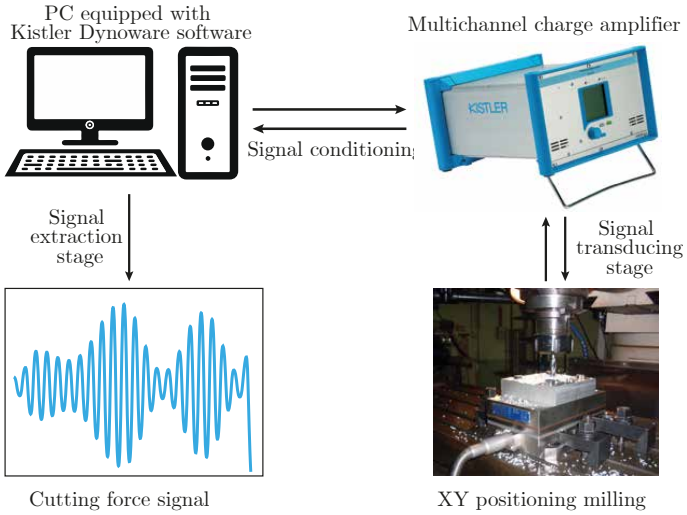

Figure 3.5: *Schematic diagram for cutting force characterization*

Figure B.1, illustrates the mounting points of the Kistler Dynamometer; Point 1 to 4, and the Aluminium block is further mounted again on the Dynamometer with M8×35mm at the edges. The Dynamometer was connected to the charge amplifier in combination with the DAQ board. The personal computer was furnished with Kistler Dynoware[3] software acting as a data acquisition unit and the cutting forces were measured as a function of time.

Additionally, the Aluminium block dimension was 100 mm×100 mm×25 mm. The sandwiched configuration of the Dynamometer as shown in Figure 3.6, ensured

[3] https://www.kistler.com/INT/en/cp/software-dynoware-2825a/P0000205

a rigid structure there by eliminating unnecessary vibrations which could lead to inaccurate data and uneven distribution of forces. Additionally, Figure 3.7, illustrates the cutting force outline during the milling process both from side and top view.

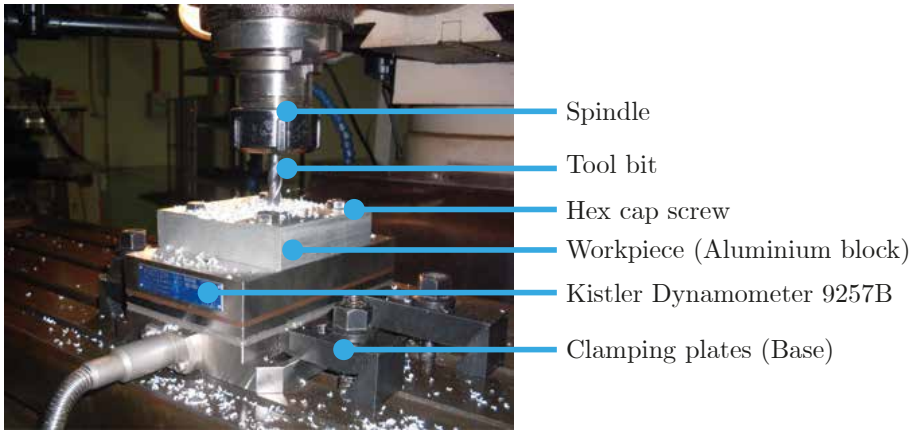

Figure 3.6: *Aluminium block during milling operation*

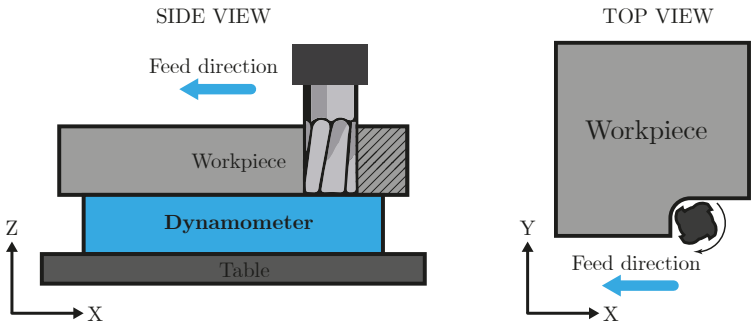

Figure 3.7: *An overview of cutting force during milling process*

3.5.2 Characterization of measured cutting force

In the process of cutting force characterisation, the task is broken up into two steps which involves firstly the selection of parameters, followed by the design of the cutting path. In the first task, the cutting forces are dependent on parameters including; feed rates, depth of cut and spindle speed. The recommended parameters as shown in Table 3.3, as suggested by [Serope Kalpakjian, 2020], provides a general range for milling operation. More details are presented in Appendix D.

Table 3.3: *Recommended cutting parameters for Aluminium workpiece*

Material	Feed (mm/tooth)	Spindle speed (rpm)	Depth of cut (mm)
Aluminium (Al)	0.08 - 0.46	300 - 3000	1.0 - 8.0

The chosen parameters in this thesis was based on [Maharof et al., 2020] which was 1500 rpm, 2500 rpm and 3000 rpm. Additionally all the other remaining parameters where kept constant. However, the feed rate was calculated using Equation (2.3), as shown in the example in Appendix C. Finally, the final cutting parameters applied in the processes are shown in Table 3.4.

Table 3.4: *Cutting parameters in experimental design*

Expt. No	Feed (mm/tooth)	Feed rate (mm/min)	Spindle speed (rpm)	Depth of cut (mm)
1	0.2	1200	1500	1.0
2	0.2	2000	2500	1.0
3	0.2	2800	3000	1.0

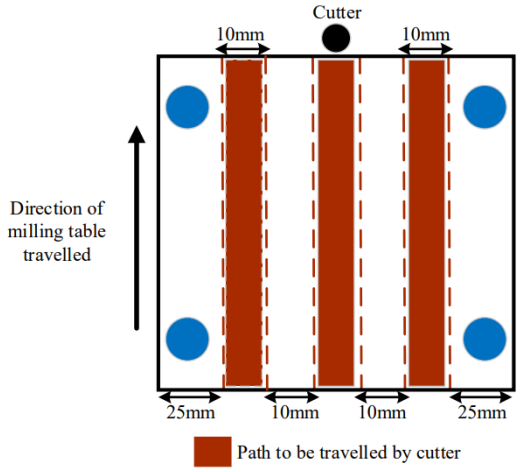

Figure 3.8: *Cutting path for force measurement [Maharof et al., 2020]*

Regarding the path of the cutting operation, straight-line cuts of 10mm width, and three columns were performed as shown in Figure 3.8. The three different

columns where carried out independently at different spindle speeds; that is, 1500 rpm, 2000 rpm and 3000 rpm respectively. The resultant cutting forces recorded against time is shown in Figure 3.9 for 1500 rpm spindle speed. It shows that the first two seconds showed null value (air cutting process) meaning no material removal was performed on the workpiece. After two seconds we observe a magnitude force in the cutting zone due to the interference between the tool and the Aluminium block.

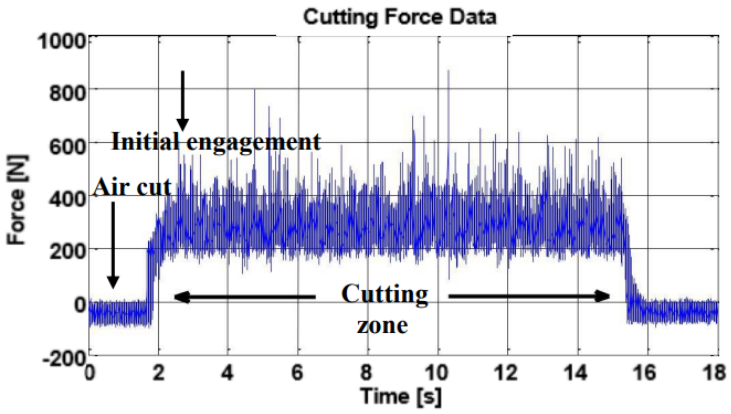

Figure 3.9: *Measured cutting force signal at 1500 rpm spindle speed [Maharof et al., 2020]*

3.5.3 Profiling of the measured cutting forces

After the measurement of the function is terminated, it needs to be converted to the proper units for numerical analysis. The measured forces were in Newtons (N). However, the transfer function expresses relation between the output (displacement in mm) and the input (Voltage in Volts). In contrast to the architecture of the block diagram, the cutting force is are designed as disturbance input to the system. To achieve this‘disturbance (represented as voltage), a conversion factor is used as described in Section 3.4, which has a magnitude of 1/2871.14 V/N. Figure 3.10, illustrates a MATLAB/Simulink equivalent diagram with the block conversion factor applied to the input as disturbance.

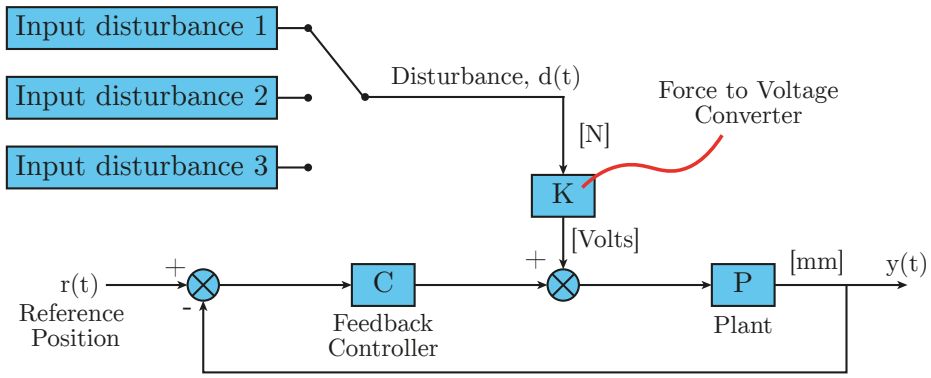

Figure 3.10: *Insertion of measured cutting forces into the control system*

3.5.4 Analysis and interpretation of measured cutting forces

The collection and measurement of the cutting forces are obtained in the time domain. Similarly, the analysis of these cutting forces are desired to be analysed in the frequency domain. Thus, Fast Fourier Transform (FFT) methods is used to convert the recorded forces from time to frequency domain, which allows and provide more visualization on the frequency characteristics of the cutting forces. Examining spectral the content of signals, permits valuable insights into the behaviour of the system with respect to various spindle speeds.

As shown in Figure 3.11, the spectral analysis display the frequency content of the cutting forces at different spindle speeds is obtained. In order to avoid unnecessary vibration and inaccuracies in the machine tool, the high frequencies have to be compensated by the controller to improve its performance. The highest peak value of the cutting forces with respect to different frequencies at distinct spindle speed is represented by P1, P2 and P3 as in Figure 3.11, which is summarized in Table 3.5.

Table 3.5: *Cutting forces amplitudes at different spindle speeds*

Circled point	**Frequency (Hz)**	**Cutting Force (N)**
P1 (1500 rpm)	26.00	7.98
P2 (2500 rpm)	39.00	10.66
P3 (3000 rpm)	51.33	10.52

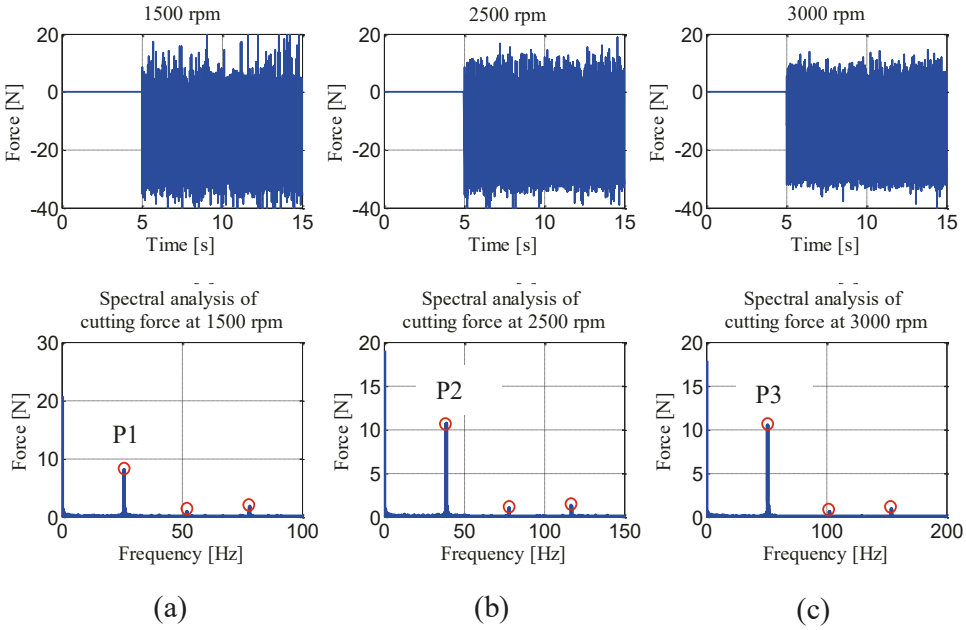

Figure 3.11: *FFT of cutting forces at (a) 1500 rpm, (b) 2500 rpm and (c) 3000 rpm spindle speed rotation*

The results displayed on Table 3.5, put in evidence a nonlinear behaviour of the cutting force due to the increase of the spindle speed rotation. The nonexistence of the relationship between spindle speed and magnitude of cutting forces explains that the higher order harmonics of spindle speeds excited the frequency correlated with the cutting process. This excitation is transported to the chip load, which is consequently reflected to the cutting force spectrum. This outcome aligns with the research conducted by cite [Ehmann et al., 1997].

3.6 Summary

The research work's approach is covered and explained in this chapter. Firstly, the experimental setup was presented, together with thorough explanations of the schematics showing the different system and data setups. An XY positioning milling table with a ball screw-driven mechanism that mirrored the basic design of a CNC milling machine made up the experimental configuration. The system was determined to be a second order system with time delay, and utilizing the non-linear least square (NLLS) frequency domain identification technique, the transfer function of the system was modeled and estimated based on the measured FRF. The servo drive's position in millimeters is related to the input voltage by means

of the transfer function. The motor constant of the ball screw driven system that converted cutting force data from Newton to volt was also identified. This was required in order to be synchronized with the system's transfer function for the purpose of numerical analysis. During the numerical analysis, the input disturbance signal took the form of a sinusoidal signal that replicated the cutting forces that were recorded. As a result, any value utilized needs to match the cutting force's actual measured magnitude. This chapter also goes into great detail on the procedures used to characterize cutting force and then analyze its spectrum. The frequencies of interest associated with the spindle speed rotation are found through the spectrum analysis. This important information is necessary for the controller design of the positioning system to be implemented successfully and efficiently. These frequencies form the basis of the observer's design. In order to ensure good tracking performance of the positioning system, the next chapter goes into depth about the design of a classical position (PID and Cascade P/PI) and robust controller (SMC) . The purpose of these control algorithms is to compensate for the high frequency content that existed in the cutting force of the milling process.

Chapter 4

CONTROLLER DESIGN

4.1 Introduction

Designing a perfect control algorithm will play a role in the compensation and reduction of the disturbance forces present in the electromechanical linear stage of the CNC machine. This is designed in order to achieve robustness, stability and accuracy in the machining process. This chapter presents the design analysis of the discussed controllers, i.e, (i) PID, (ii) cascade P/PI and (iii) Sliding Mode Control (SMC).

4.2 Design and Analysis of PID controller

The control strategy of PID controller makes it very popular and prominently applied in machine tool technology. Laying its basis on Proportional (P), Integral (I) and Derivative (D), the basic control diagram that is related to the proposed controller is shown in Figure 2.16, and its general transfer function $G_{PID}(s)$ is expressed as;

$$PID(s) = K_p + \frac{K_i}{s} + K_d \cdot s \tag{4.1}$$

Next, the open and closed loop transfer function are examined based on the scheme. Thus the open and closed loop transfer functions are;

$$G_{pid.OL}(s) = \frac{Y(s)}{R(s)} = G_c(s) \cdot G_p(s) \tag{4.2}$$

$$G_{pid.CL}(s) = \frac{G_{pid.OL}(s)}{1 + G_{pid.OL}(s)} \tag{4.3}$$

The PID controller here is designed using traditional open loop shaping followed by closed loop tuning in frequency domain. However, The design criteria was based on open loop and closed loop properties of the adequate transfer functions. These include phase margin (PM), Gain margin (GM), Nyquist stability and bandwidth of the control system.

The parameters K_p, K_i and K_d were selected based on the gain and phase margin of the open loop transfer function. [Sigurd Skogestad, 2005] requires a $GM > 2$ and $PM > 30°$. To ensure performance and disturbance rejection, the considered parameters are gain margin (6 - 10 dB) and phase margin (30 - 60°).

In total 3 sets of PID gains where tuned, where it also displays the respective gain and phase margins of the open loop transfer function as listed in Table 4.1. However, Design 3 was based on Ziegler Nicolas Tuning Method which is a classical tuning rule.

Ziegler-Nichols' give a system closed-loop with smaller stability margins and a more oscillatory response than would normally be regarded as acceptable. For disturbance rejection the controller settings may be more reasonable, and one can add a prefilter like a Notch filter to improve the response for reference tracking, resulting in a two degrees-of-freedom controller [Sigurd Skogestad, 2005]. However, this will not change the stability robustness of the system

Table 4.1: *PID gain values Kp, Ki and Kd, with respective Gain and Phase margins for three different designs*

Parameter	**Design 1**	**Design 2**	**Design 3**
K_p **(V/mm)**	0.9447	1.2764	1.0773
K_i **(V/mm · s)**	43.6659	59.0000	122.4930
K_d **(V · s/mm)**	0.0042	0.0057	0.0024
Gain Margin (GM)	11.7 dB (at 202 Hz)	9.13 dB (at 202 Hz)	15.1 dB (at 173 Hz)
Phase Margin (PM)	56.5° (at 53 Hz)	51.4° (at 71.1 Hz)	22.4° (at 43.1 Hz)

Figure 4.1 to 4.3, displays the Bode diagram of the velocity open loop transfer function. Accompanied to that, the Nyquist plot (each drawn with a unit circle) also verified the open loop stability of the transfer function, where there was no encirclement around the location [-1, 0]. Thus, the open loop was stable.

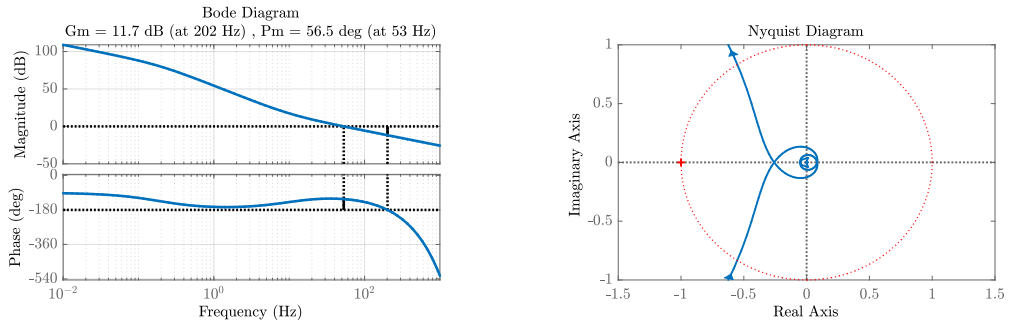

(a) ***(b)***

Figure 4.1: *(a) Bode diagram of open loop transfer function with gain margin of 11.7 dB at 202 Hz and phase margin of 58.5° at 53 Hz (b) Nyquist plot of the open loop transfer function of Design 1.*

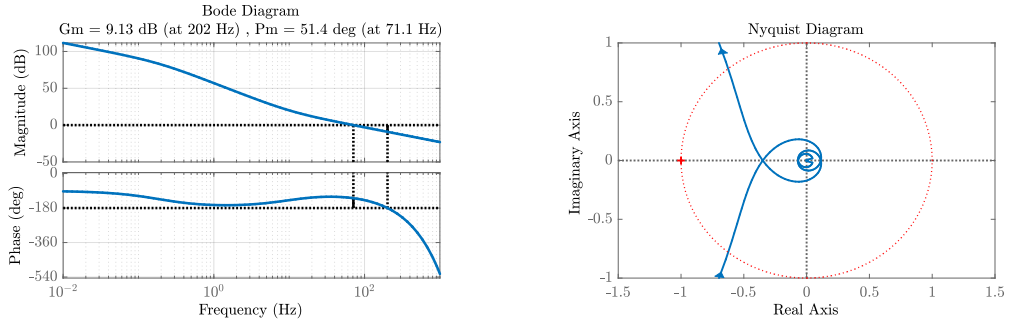

(a) ***(b)***

Figure 4.2: *(a) Bode diagram of open loop transfer function with gain margin of 9.13 dB at 202 Hz and phase margin of 51.4° at 71.1 Hz (b) Nyquist plot of the open loop transfer function of Design 2.*

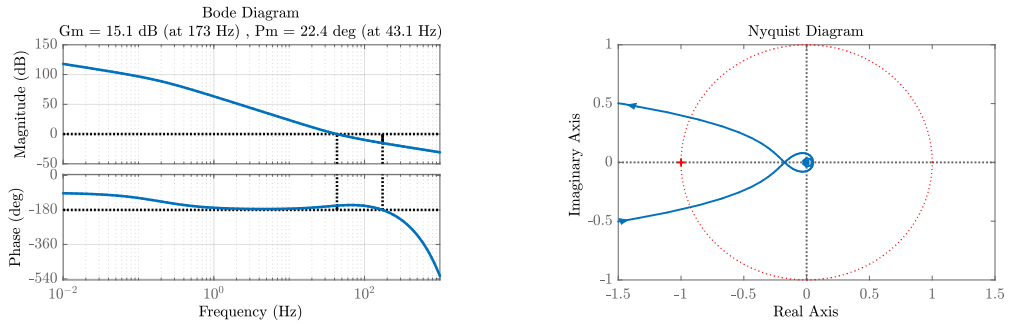

(a) *(b)*

Figure 4.3: *(a) Bode diagram of open loop transfer function with gain margin of 15.1 dB at 173 Hz and phase margin of 22.4° at 43.1 Hz (b) Nyquist plot of the open loop transfer function of Design 3.*

4.2.1 PID controller analysis in time domain

The designed set of gains similarly based on gain and phase margin was analysed using step response for much more detailed inclination on the optimal controller for the system. As discussed in the literature in Section 2.6.2. It was analyzed using the Steady state error, Rise time (T_r), Settling time (T_s) and Percentage overshoot, ($\%OS$). This provides also good intuition on how the response of different controllers will react based on a unit step input. Figure 4.4(a), 4.4(b) and 4.4(c), shows the step response for Design 1, Design 2 and Design 3 with their respective step response characteristics, respectively.

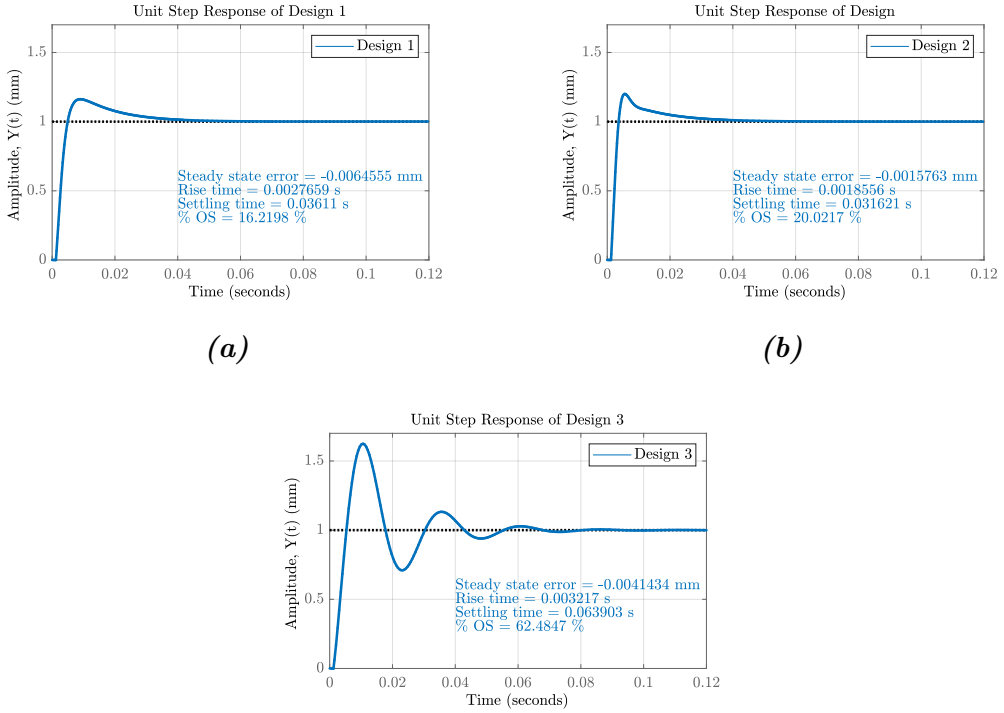

Figure 4.4: *Step response analysis of (a) Design 1 (b) Design 2 (c) Design 3.*

4.2.2 PID controller Selection

Based on the frequency and time domain in the above sections, It was important to select the supposed best gains that will meet the robustness and disturbance criteria, which will further be validated in the next section.

From the Bode plot analysis we observe that Controller Design 3 (see Figure 4.3), has higher gain margin which is desirable for robust performance. However, its phase margin was 22.4 deg which is below 30 deg as the standard recommended value for disturbance rejection. This lower phase margin produces oscillations and higher overshoots in the output step response caused by the marginal stability. This is put in evidence in step responds plot illustrated in Figure 4.4(c).

Comparing Design 1 and Design 2, both produced very desirable phase and gain margins. However, Design 1 had its phase margin 1.7 deg higher than the range that the design lay its basis on. That is acceptable but did not match our design requirements.

With that said Design 2, was chosen to be the final PID controller design. The following parameter that was determined is the magnitude plot of the sensitivity

function $S_{pid}(s)$ which is denoted in Equation (2.11). The bandwidth is then defined as the frequency at which the magnitude of the sensitivity function crosses the -3 dB line from below. Figure 4.5, shows the sensitivity function of the transfer function where the bandwidth is displayed to be 33.2 Hz Similarly Figure 4.6 displays the bode diagram of the closed loop transfer function. A highly sensitive system would be vulnerable to input disturbance input, thus, it is desired to obtain a low sensitive system due to the design controller to ensure robustness.

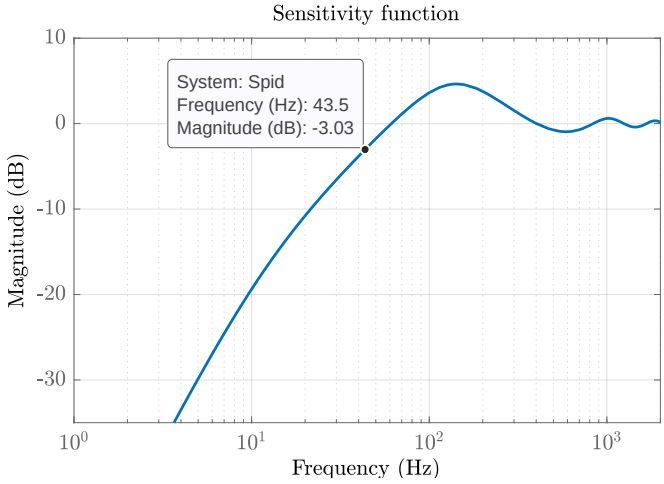

Figure 4.5: *Sensitivity Function of PID controller*

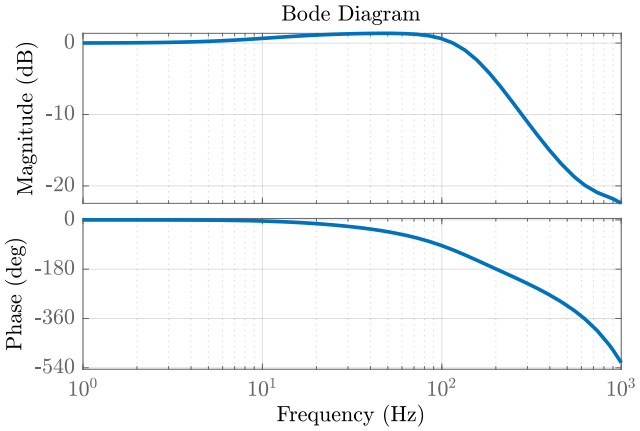

Figure 4.6: *Bode Diagram of closed loop transfer function*

4.2.3 PID Controller Design Validation

The good tracking performance and disturbance force rejection of the selected PID was necessary to be assessed to ensure its validity. As the control scheme was simulated by providing a sinusoidal reference input of 5 mm amplitude and 0.5 Hz frequency in Simulink as shown in Figure 4.8. The system transfer function was excited where the position tracking error where measured and distinguished magnitude value obtained from the controller error transfer function, $E(s)$ from Equation (2.8), The amplitude of the tracking errors corresponds to the magnitude of the error transfer function $E(s)/R(s)$ (see Equation (2.8)) with $D(s) = 0$ and $N(s) = 0$. As shown in Figure 4.7 where the simulated tracking error was tightly equal to the error transfer function at the oscillation frequency; the results recorded was around 1.8547 μm and 1.85 μm respectively.

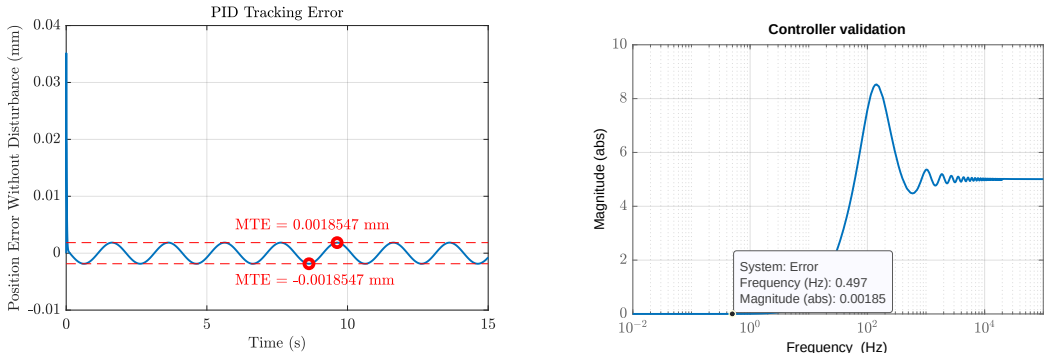

(a) *(b)*

Figure 4.7: *(a) Simulated tracking error of the sinusoidal reference signal of an amplitude of 5 mm and frequency 0.5 Hz, and (b) PID position error transfer function.*

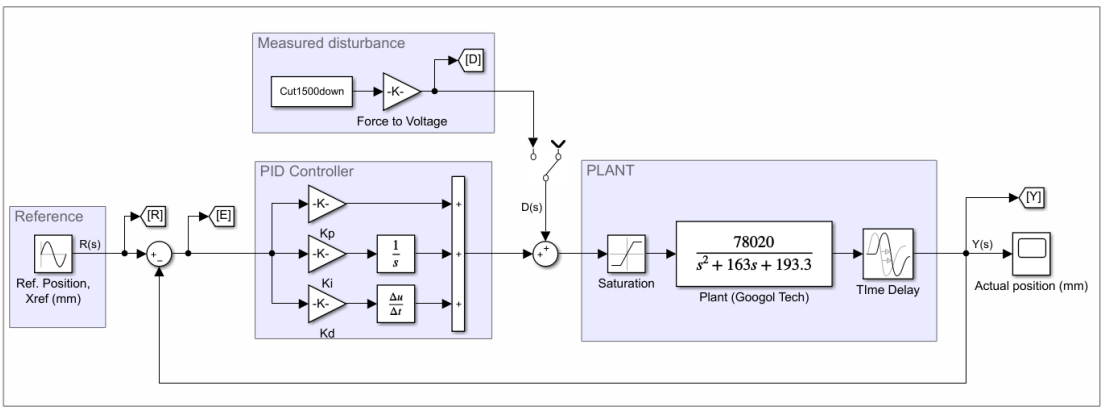

Figure 4.8: *Simulated Simulink Block diagram of PID controller*

4.3 Design and Analysis of Cascade P/PI controller

One of the most common control strategy in motion control particularly in CNC machines tools is the cascade P/PI controller. It is therefore popular due to its simplicity in structure, flexible design and response effectiveness in regards to disturbance. In this thesis, the cascade controller was design by the use of loop shaping technique in the frequency domain [Jamaludin et al., 2007a] [Maharof et al., 2020] [Jamaludin et al., 2007b]. By using the gain margin, phase margin, Nyquist stability and bandwidth of the control system, the characteristics of both the open and closed loop transfer functions where examined.

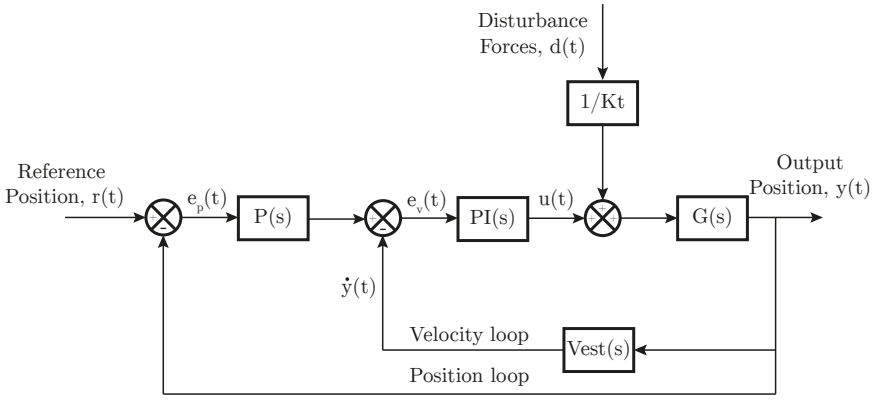

Figure 4.9: *General control scheme of a cascade P/PI structure*

In order to design the cascade P/PI controller, the control structure was broken down into two loops; Velocity and Position loop. The position loop is built over the velocity loop as illustrated in Figure 4.9. The reference position input and output position are indicated as $r(t)$ and $y(t)$ respectively. The velocity signal is obtained from V_{est} transfer function, which could also obtain from direct differentiation. The velocity controller is composed of the Proportional-Integral (PI) controller, while the position controller only consist of a Proportional (P) controller.

4.3.1 Design and Analysis of the Velocity Loop

The velocity loop of the cascade P/PI control schemes is comprised of only the PI velocity controller. $V_{est}(s)$ estimates the velocity from the position signal coming from the encoder. The general equation making the PI controller is as follows;

$$PI(s) = K_p + \frac{K_i}{s} \tag{4.4}$$

Where, K_v and K_i are the proportional gain and integral gain of the velocity loop respectively.

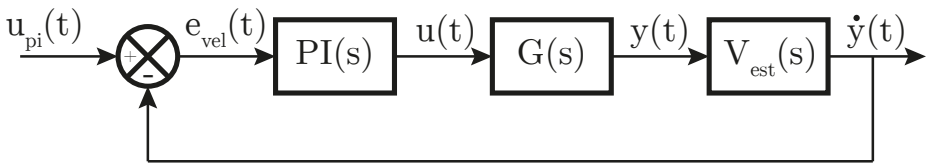

Figure 4.10: *Block diagram representation of Velocity loop*

The block diagram of the velocity control loop is illustrated in Figure 4.10. By using the loop shaping technique, the analysis of the open loop, $V_{ol}(s)$ and closed loop V_{cl} transfer functions where determined and analysed as follows;

$$V_{ol} = \frac{\dot{Y}(s)}{E_{vel}(s)} = PI(s) \cdot G(s) \cdot V_{est}(s) \tag{4.5}$$

$$V_{cl} = \frac{V_{ol}(s)}{1 + V_{ol}(s)} = \frac{PI(s) \cdot G(s) \cdot V_{est}(s)}{1 + PI(s) \cdot G(s) \cdot V_{est}(s)} \tag{4.6}$$

$$\text{Where, } V_{est} = \frac{942.5s}{s + 942.5} \tag{4.7}$$

The compliance function, $\frac{Y(s)}{D(s)}$ and the sensitivity function, $S_v(s)$ of the velocity loop are;

$$\frac{Y(s)}{D(s)} = \frac{G(s)/K_t}{1 + PI(s) \cdot G(s) \cdot V_{est}(s)} \tag{4.8}$$

$$S_v(s) = \frac{1}{1 + V_o l(s)} = \frac{1}{1 + PI(s) \cdot G(s) \cdot V_{est}(s)} \tag{4.9}$$

By using the Matlab SISO tool for tuning, the K_v and K_i were design and selected based on the gain and phase margin consideration of the open loop transfer function. The selected criteria was chosen such that Gain margin (4 dB - 6 dB) and the Phase margin (40 - 60 deg) provides a good stability and transient response performance. Table 4.2, then shows the list of PI control parameters and also the corresponding gain and phase margin.

Table 4.2: *Velocity loop PI controller parameters and corresponding Gain margin and Phase margin*

$K_v(Vs/mm)$	0.00385
$K_i(Vs^2/mm)$	0.20001
Gain margin	11 dB (at 131 Hz)
Phase margin	79.7 deg (at 39.5 Hz)

Table 4.2, shows the resulting gain and phase margin of the velocity open loop. These thus ensures good characteristics performance for the velocity loop. Figure 4.11, shows the Bode diagram of the velocity open loop transfer function. Similarly, Figure 4.12, shows the Nyquist plot confirming the stability of the velocity loop by non encirclement at [-1, 0] coordinate.

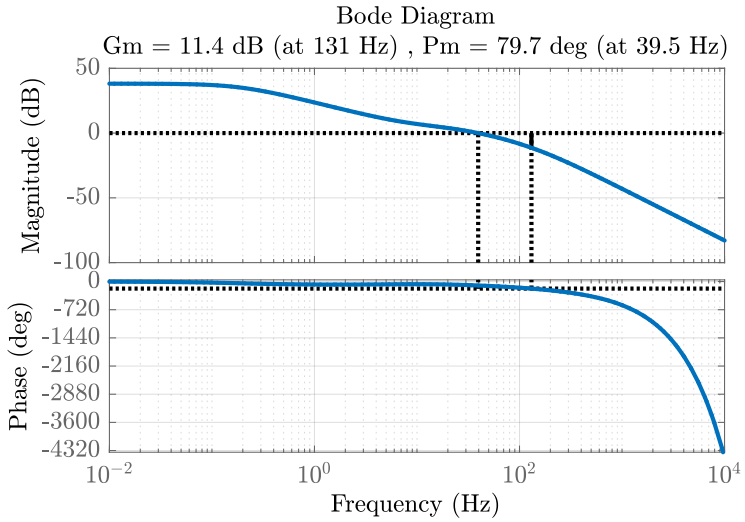

Figure 4.11: *Bode plot of the velocity open-loop transfer function with a gain margin of 11.4 dB (at 131 Hz) and phase margin of 79.9 deg (at 39.5 Hz)*

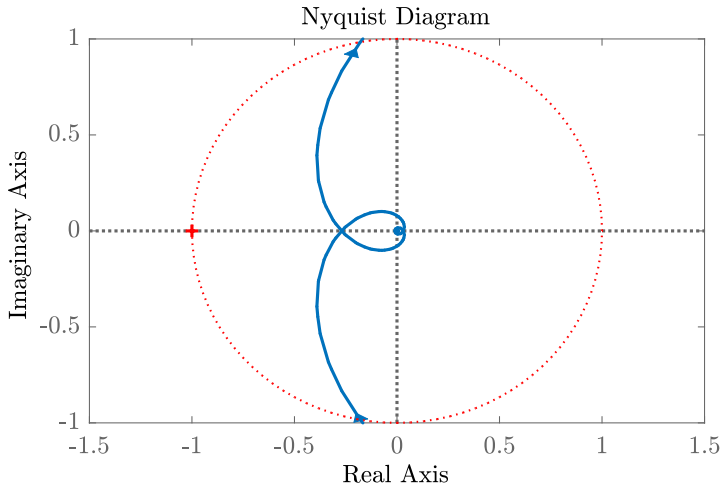

Figure 4.12: *Nyquist diagram of the velocity open-loop transfer function*

Furthermore, the bandwidth of the velocity loop was determined from the magnitude of the sensitivity function, $S_v(s)$ from Equation (4.9). Thus the bandwidth was determined at 35.2 Hz using the -3 dB reference as shown in Figure 4.13. The sensitivity function quantify how well the velocity controller can reject disturbance

and attenuate noise. A low sensitivity indicates the ability to maintain good reference despite the presence of input disturbance, thus ensuring robustness. This is a more accurate representation of system performance compared to traditional complimentary sensitivity function from Equation (4.9), [Sigurd Skogestad, 2005]. The bode diagram of the velocity closed loop transfer function is shown in Figure 4.6.

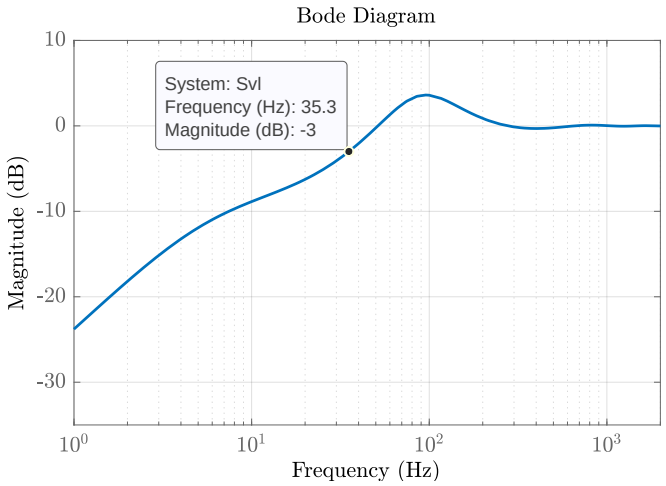

Figure 4.13: *Sensitivity function of the velocity loop*

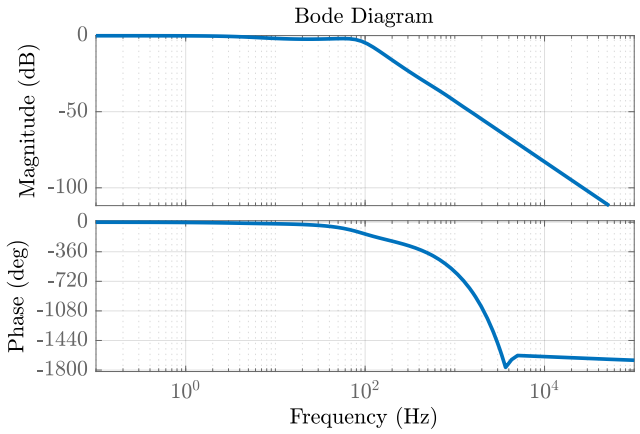

Figure 4.14: *Bode diagram of velocity closed-loop transfer function*

4.3.2 Design and Analysis of the Position Loop

After designing the velocity loop, the next step required to produce the complete cascade control scheme is to design the position loop. This consist of a Proportional (P) controller that builds on over the velocity loop. The position open and closed loop are analysed for proportional gain K_p as follows;

$$P = K_p = 359.18\, s^{-1} \tag{4.10}$$

The proposed consideration was such that Gain margin and phase margin was at least 5 dB and 30 degree respectively. The open and closed loop position transfer function are formulated as follows;

$$P_{ol} = \frac{Y(s)}{Ep(s)} = \frac{P(s) \cdot PI(s) \cdot G(s)}{1 + PI(s) \cdot G(s) \cdot V_{est}(s)} \tag{4.11}$$

$$P_{cl} = \frac{Y(s)}{R(s)} = \frac{P(s) \cdot PI(s) \cdot G(s)}{1 + PI(s) \cdot G(s) \cdot V_{est}(s) + P(s) \cdot PI(s) \cdot G(s)} \tag{4.12}$$

Additionally, the compliance and sensitivity function were formulated as follows;

$$\frac{R(s)}{D(s)} = \frac{G(s)/K_t}{1 + 1 + PI(s) \cdot G(s) \cdot V_{est}(s) + P(s) \cdot PI(s) \cdot G(s)} \tag{4.13}$$

$$S_p(s) = \frac{1}{1 + P_{ol}(s)} = \frac{1}{1 + PI(s) \cdot G(s) \cdot V_{est}(s) + P(s) \cdot PI(s) \cdot G(s)} \tag{4.14}$$

In order to validate and confirm the tracking performance based, position steady-state error transfer function was used and visualised as a function of frequency. The position steady-state error transfer function, $Ep(s)$ equals;

$$Ep = A \cdot R(s) - B \cdot D(s) \tag{4.15}$$

where,

$$A = \frac{1 + PI(s) \cdot G(s) \cdot V_{est}(s)}{1 + PI(s) \cdot G(s) \cdot V_{est}(s) + P(s) \cdot PI(s) \cdot G(s)}$$

$$B = \frac{G(s)/K_t}{1 + 1 + PI(s) \cdot G(s) \cdot V_{est}(s) + P(s) \cdot PI(s) \cdot G(s)}$$

The gain margin and phase margin was identified and are shown in Figure 4.15, which is further summarised in Table 4.3. The magnitude of of the gain margin and phase margin was 5.16 dB (at 83.7 Hz) and 46.3 deg (at 47.6 Hz) respectively. This ensured good system stability and transient responds. As shown in Figure 4.16, the Nyquist plot of the position open loop transfer function was not encircled

at [-1, 0] which confirms the system stability. The bode plot of the position closed loop transfer function is also shown in Figure 4.17.

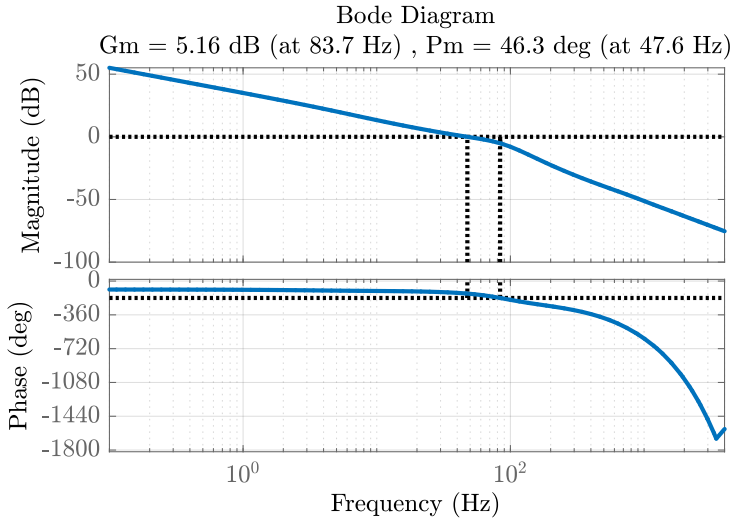

Figure 4.15: *Bode plot of the position open-loop transfer function with a gain margin of 5.16 dB (at 83.7 Hz) and phase margin of 46.3 deg (at 47.6 Hz)*

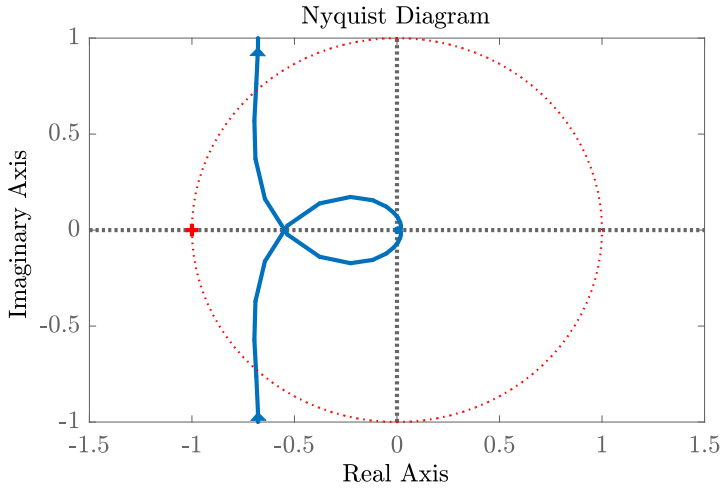

Figure 4.16: *Nyquist diagram of the position open-loop transfer function*

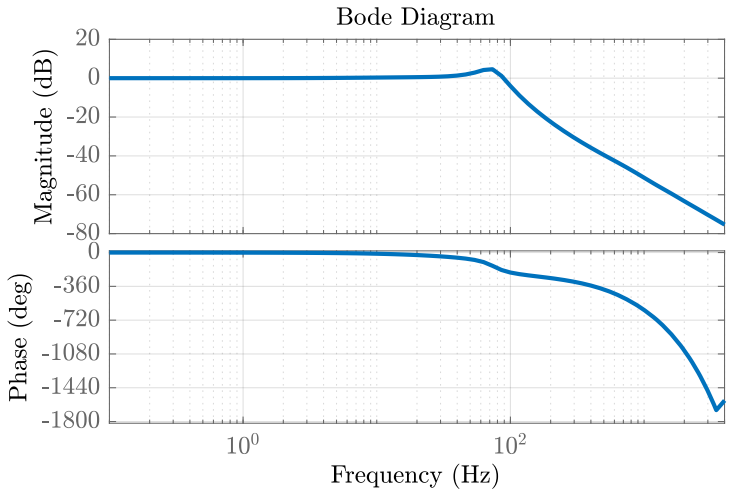

Figure 4.17: *Bode diagram of position closed-loop transfer function*

Table 4.3: *Position loop P controller parameters and corresponding Gain margin and Phase margin*

$K_p(Vs^{-1}/mm)$	359.18
Gain margin	5.16 dB (at 83.7 Hz)
Phase margin	46.3 dB (at 47.6 Hz)

The next step was to determine the bandwidth of the position loop from the -3 dB crossing from below from the sensitivity function $S_p(s)$, see Equation (4.14). Figure 4.18, illustrates the sensitivity function plots with bandwidth equals 28.7 Hz.

The peaks of the sensitivity magnitude curves lie slightly above the conventional recommendation of 6 dB (or Abs. value 2) [Sigurd Skogestad, 2005]. This was acceptable for the system peak value observed at a frequency of 74.1 Hz as shown in Figure 4.19. Also, the results of Table 4.4, confirm the fundamental characteristics of a cascade controller, that is, the bandwidths of the position loop is smaller than the bandwidth of the inner velocity loop.

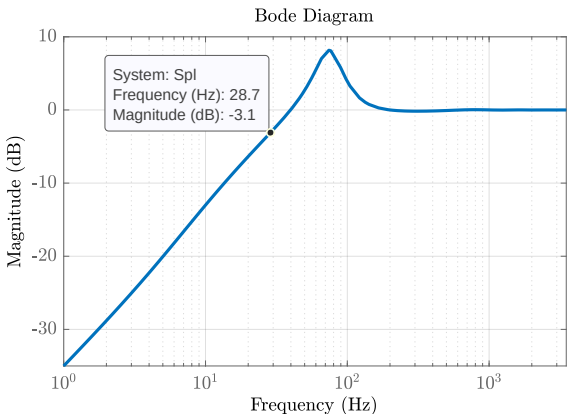

Figure 4.18: *Sensitivity function of the position loop*

Table 4.4: *Bandwidths of Velocity and Position Loops*

Loop	Velocity	Position
Bandwidth	35.3 Hz	28.7 Hz

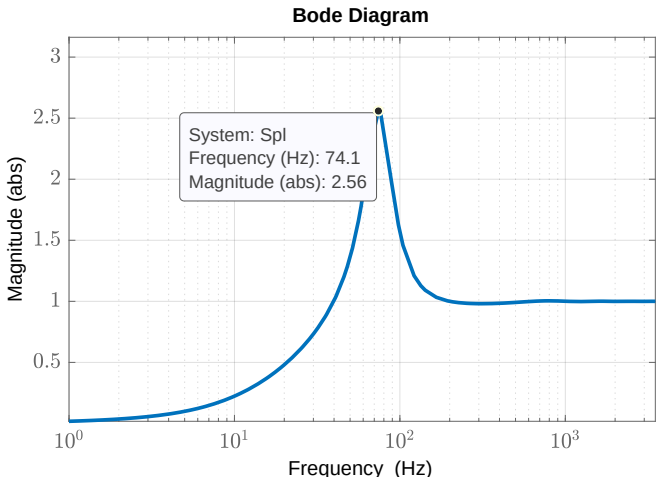

Figure 4.19: *Peak Value sensitivity of the position loop at Abs. 2.56 at 74.1 Hz*

4.3.3 Cascade controller design validation

A good tracking performance on the designed controller was evaluated by using the position and tracking errors. Similarly to Section 4.2.3, the tracking perfor-

mance of cascade P/PI controller is examined for thesame sinusoidal reference signal. With a sinusoidal reference signal of amplitude 5 mm and frequency 0.5 Hz, The position errors where calculated and compared with theoretical values obtained from magnitude of error transfer function, $E_p(s)$ in Equation (4.15), with $D(s) = 0$ and $N(s) = 0$. As shown in Figure 4.20, the simulated tracking error was tightly equal to the error transfer function at the oscillation frequency; the results recorded was around 0.04425 mm and 0.0452 mm respectively. The Simulink Block diagram is shown in Figure 4.21.

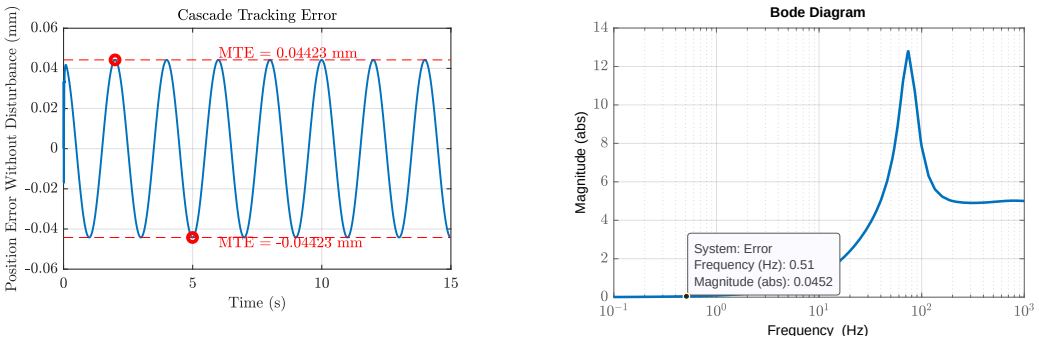

(a) *(b)*

Figure 4.20: *(a) Simulated tracking error of the sinusoidal reference signal of an amplitude of 5 mm and frequency 0.5 Hz, and (b) Cascade position error transfer function*

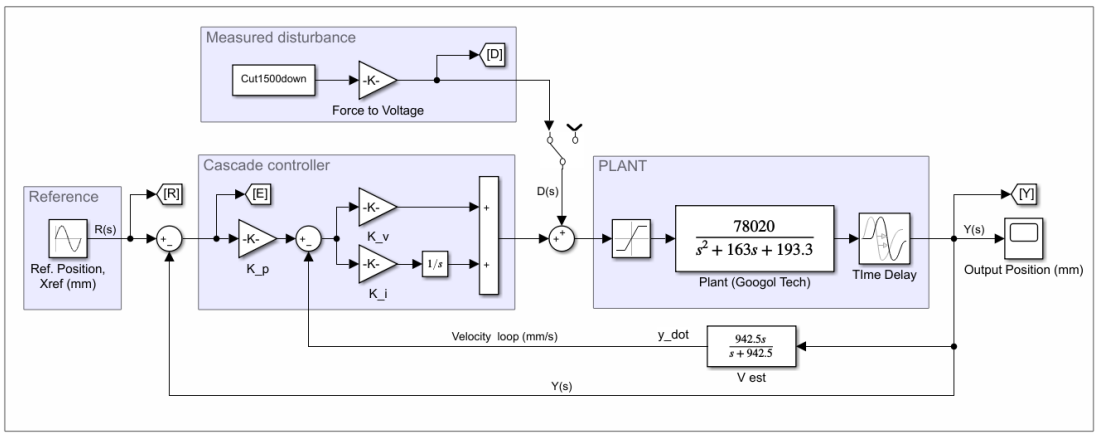

Figure 4.21: *Simulated Simulink Block diagram of Cascade controller*

4.4 Design and Analysis of SMC controller

The block diagram of a general sliding mode control scheme is shown in Figure 4.22. The block diagram accepts reference input R(s) and actual output Y(s). The disturbance D(s) and control law U.

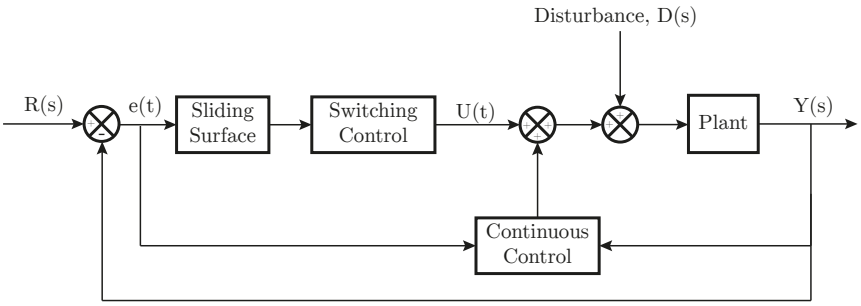

Figure 4.22: *General block diagram representation of Sliding Mode Control*

The fundamental(Classical) Sliding Mode Control design consist of two parts which are; continuous control law, $U_c(t)$ (sliding surface) and the discontinuous control law, $U_d(t)$ (switching function). The sliding surface, $S(t)$, thus dependent on the error and time derivative is express as follows;

$$s(e, \dot{e}) = \left(\frac{d}{dt} + \lambda\right)^{n-1} \cdot e(t) \tag{4.16}$$

$$e(t) = y(t) - r(t) \tag{4.17}$$

For second order transfer function, $n = 2$, where the sliding surface becomes,

$$s(t) = \dot{e} + \lambda e \tag{4.18}$$

After the sliding surface of the SMC was selected, the control law $U(t)$, at the moment of approaching the sliding surface, the switching function is equivalent to zero. The control law is then expressed as;

$$U(t) = U_c(t) + U_d(t) \tag{4.19}$$

The discontinuous law consist of a signum function denoted by

$$U_d(t) = -K \cdot sgn(s) \tag{4.20}$$

The design proceeded with the establishment of the continuous control law. Considering the transfer function $G_s(s)$ as in Equation (4.21), and taking the inverse laplace transform we obtain Equation (4.22)

$$\frac{Y(s)}{U(s)} = \frac{78020 \cdot e^{-0.0012s}}{s^2 + 163s + 193.3} \tag{4.21}$$

$$78020U(t) = \ddot{y} + 163\dot{y} + 193.3y \tag{4.22}$$

The derivative of Equation (4.18), is given in Equation (4.23) and substituting $\ddot{e} = \ddot{y} - \ddot{r}$ gives Equation (4.24). Furthermore solving Equation (4.22), for the highest-order differential term, and putting in Equation (4.24), the new derivative of the sliding surface was obtained as in Equation (4.25).

$$\dot{s} = \ddot{e} + \lambda\dot{e} \tag{4.23}$$

$$\dot{s} = \ddot{y} - \ddot{r} + \lambda\dot{e} \tag{4.24}$$

$$\dot{s} = 78020U(t) - 163\dot{y} - 193.3y - \ddot{r} + \lambda\dot{e} \tag{4.25}$$

The continuous control law occurs when $\dot{s} = 0$. Thus the continuous controller $U_c(t)$ is obtained as;

$$U_c(t) = \frac{1}{78020}(163\dot{y} + 193.3y + \ddot{r} - \lambda\dot{e}) \tag{4.26}$$

Finally, as denoted in Equation (4.19), the SMC control input law is written as;

$$U(t) = \frac{1}{78020}(163\dot{y} + 193.3y + \ddot{r} - \lambda\dot{e}) - K \cdot sgn(s) \tag{4.27}$$

This equation was used as the basis of the control law in Simulink in order to tune the parameters, λ and K by conventional tuning methods as proposed in [Christopher Edwards, 1998a]. Based on this heuristic method, the values of λ and K equals 600 and 0.010 respectively. The resulting Simulink block diagram is illustrated as shown in Figure 4.23.

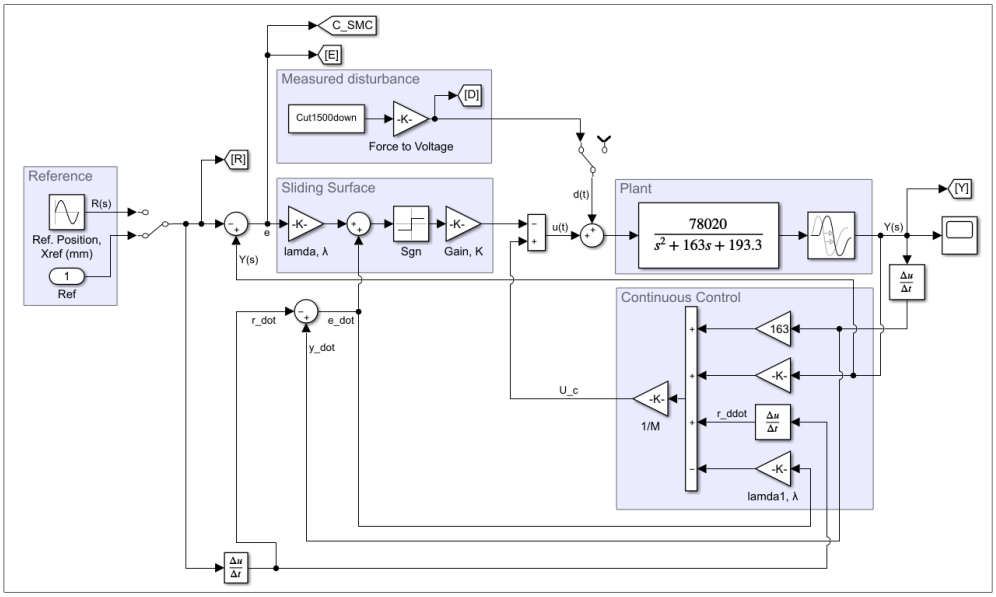

Figure 4.23: *Simulated Simulink Block diagram of Classical Sliding Mode Control.*

Design of a Sigmoid Sliding Mode Control

In the Classical SMC, the discontinuous function attached to the control input results in high switching frequency and chattering effect of the input voltage. This phenomenon is not desirable in practical implementation. A sigmoid-like function is used to substitute the discontinuous Signum function which reduces the noise content of the control input signal. The Sigmoid-like function is represented as;

$$V_\delta(s) = \frac{s}{|s| + \delta} \tag{4.28}$$

The degree of the continuous approximation is shown by the positive constant δ. Non-ideal sliding motion, sometimes referred to as pseudo-sliding, occurs when the states reside inside a defined sliding surface boundary as opposed to having an ideal sliding motion [Jamaludin et al., 2007b]. The value of δ was selected as 20. The designed Simulink structure of Sigmoid SMC is illustrated below.

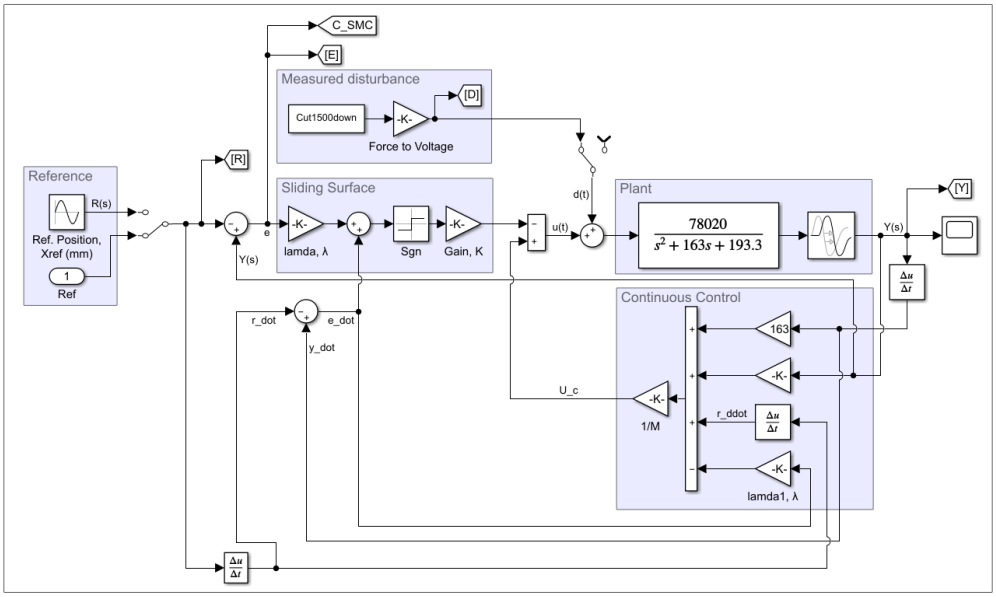

Figure 4.24: *Simulated Simulink Block diagram of Sigmoid Sliding Mode Control.*

Design of Super Twisted Sliding Mode Control

The primary objective of the design of classical SMC is to drive the sliding surface and its first order derivative to zero [Christopher Edwards, 1998b] [Utkin, 1977], $s = \dot{s} = 0$. Another popular implementation is renamed as Super Twisted Sliding Mode Control, ST-SMC. Here, the algorithm does not need to be aware of the derivative of the sliding surface, $\dot{s}$ in its structure and implementation. This is makes it easier and preferable [Levant and Levantovsky, 1993]. The ST-SMC has thesame design procedure as classical SMC. Thesame sliding surface as in Equation (4.18), and the discontinuous control law, U_d is modified which produces a new control input as stated in Equation (4.29) and (4.30).

$$U_{st}(t) = U_c - \alpha\sqrt{|s(t)|}sign(s) - u_1(t), \tag{4.29}$$

$$\dot{u}_1(t) = \beta sign(s) \tag{4.30}$$

where both α and β are positive constants.

Both parameters α and β were tuned using heuristic approach is such that the chattering effect is minimised without affecting the accuracy of the system and their respective values were 0.0024 and 0.08. The Simulink simulated block diagram of ST-SMC is illustrated in Figure 4.25, The stability is ensured by using the Lyapunov stability criterion, which was effectively demonstrated in the works of [Rubio et al., 2016] [Polyakov and Fridman, 2014].

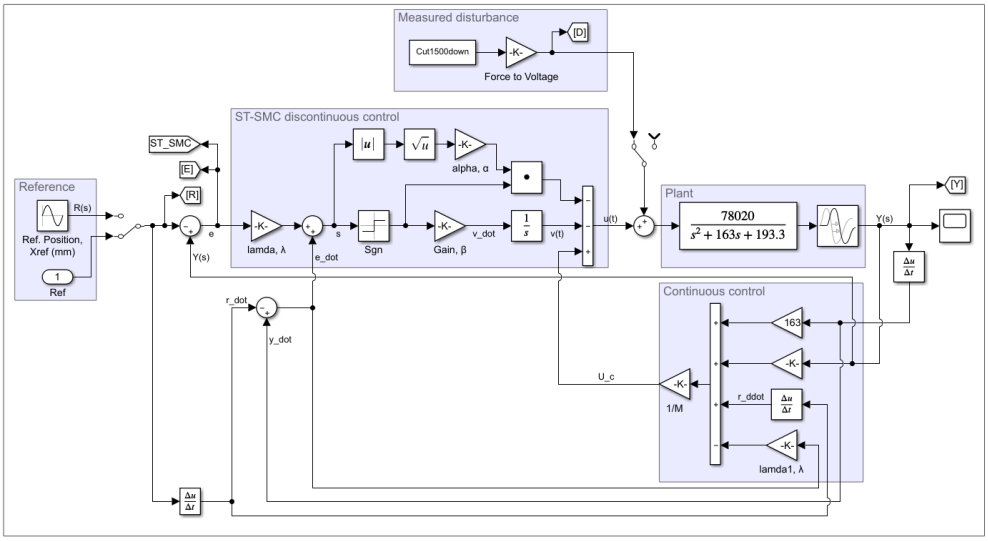

Figure 4.25: *Simulated Simulink Block diagram of Super Twisted Sliding Mode Control, ST-SMC.*

Chapter 5

RESULTS AND DISCUSSION

5.1 Numerical Performance Analysis

The numerical performance examination of this thesis was carried out for the three different suppression techniques applied in the controller design section which includes (i) PID, (ii) Cascade P/PI and (iii) SMC controller. This chapter then presents an overall display of the results accompanied with a discussion of the different techniques used accordingly. The performance Index associated with the tracking errors and disturbance rejection were based on Maximum Tracking Error (MTE), Root Mean Square Error (RMSE) and Fast Fourier Transform (FFT).

The Numerical validation was carried out in Matlab/Simulink software version 2020a and the performances were analyzed based on two cases, that is, (i) disturbance free tracking error (ii) disturbance induced tracking error. The input reference signal was chosen to be sinusoidal with amplitude of 5 mm and frequency of 0.5 Hz as shown in Figure 5.1(b). Other researchers [Maharof et al., 2020], [Jamaludin et al., 2007b], have examined the control performance with sinusoidal inputs with different harmonics to provide more information and characteristics on how the harmonics influence the tracking error.

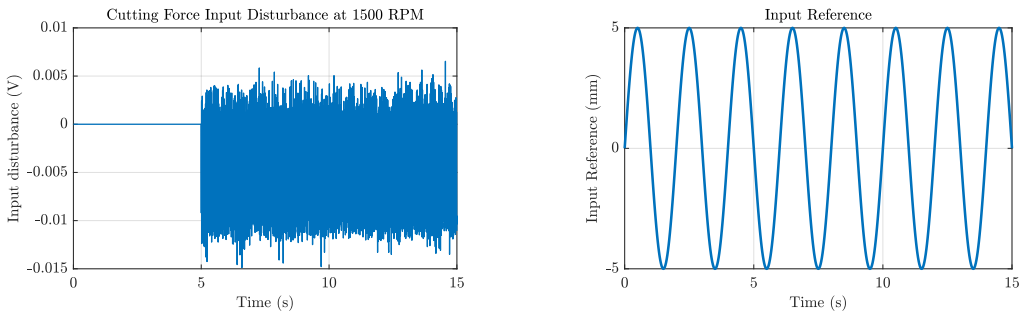

(a) ***(b)***

Figure 5.1: *(a) Cutting force input disturbance at 1500 rpm, (b) Input Reference of 5 mm amplitude and 0.5 Hz frequency.*

In regards to the time domain analysis, MTE and RMSE performance Index were used while in frequency domain, FFT was used. A single cutting disturbance force data was used throughout the evaluation and simulation, which was that with 1500 rpm spindle speed illustrated in Figure 5.1(b). Additionally, the percentage error was computed for MTE, RMSE and FFT by using the formula as follows;

$$\text{Percentage Variation} = \frac{\text{Error with disturbance} - \text{Error without disturbance}}{\text{Error without disturbance}} \times 100\% \tag{5.1}$$

5.2 Maximum Tracking Error (MTE)

This section compares the numerical results of maximum tracking errors of all the designed controller with and without input disturbance (disturbance-free and disturbance-induced).

The Results presented above illustrated that the Maximum Tracking Error for the designed PID controller for disturbance free input was 1.85 μm while that of induced disturbance was 7.04 μm, as shown in Figure 5.2.

For the cascade control structure, the MTE displayed a magnitude of 48.72 μm and 44.23 μm for disturbance free input and induced disturbance respectively. See Figure 5.3.

In regards to the SMC control structure, the MTE was recorded acording to the Classical SMC, Sigmoid SMC, ST-SMC. The Various values of the MTE of the SMC controller both with and without disturbance is summarized in Figure 5.5. The Sigmoid SMC produced the lowest value of the MTE both with and without disturbance of 1.65 μm and 0.34 μm respectively. This is shown in Figure 5.4.

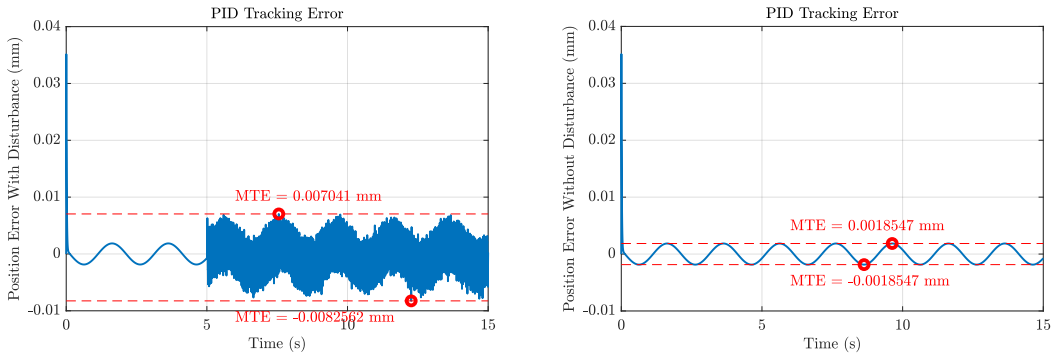

(a) ***(b)***

Figure 5.2: *PID controller MTE (a) with disturbance (b) without disturbance*

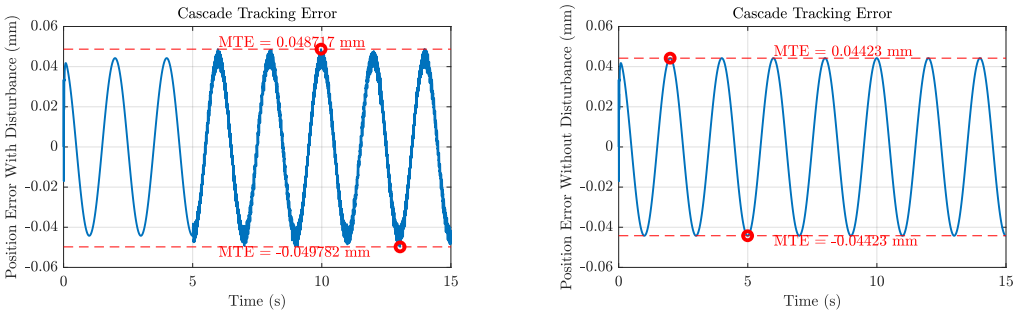

(a) ***(b)***

Figure 5.3: *Cascade P/PI controller MTE (a) with disturbance (b) without disturbance*

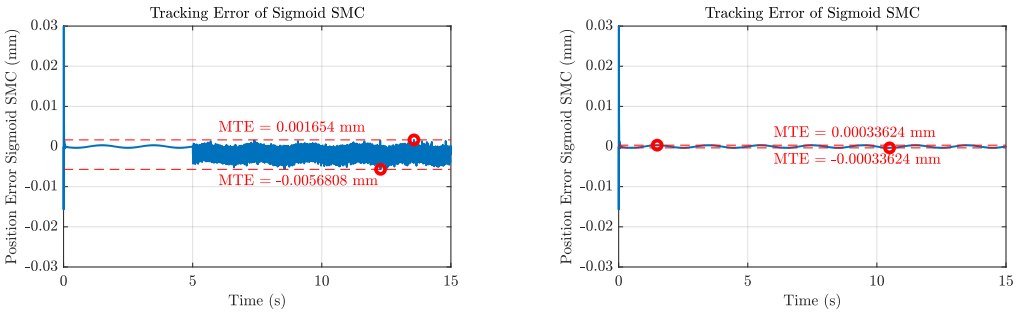

(a) ***(b)***

Figure 5.4: *Sigmoid SMC controller MTE (a) with disturbance (b) without disturbance*

From the Maximum Index performance it was clear that the Sliding Mode controller had the lowest error, followed by the PID controller. The Cascade P/PI controller showed the highest value of the error without disturbance, however its variation was less when the disturbance was injected. as observed in Figure 5.2(a), the PID observed many fluctuations with higher amplitude with respect to the input reference. Also a higher spike was observed at the beginning of the simulation, which was due to ripples in the CNC machine. On the other hand the cascade P/PI controller was able to suppress this spike which proved it to be more robust than PID. This confirms with the theoretical analysis of both the controllers.

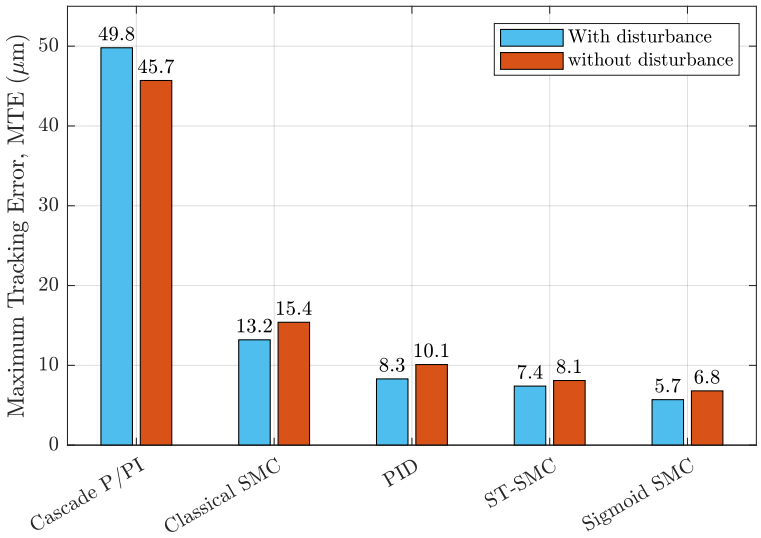

Figure 5.5: *Summary of Maximum Tracking Errors of PID, Cascade P/PI and SMC*

5.3 Root Mean Square Error (RMSE)

The Root Mean Square Error is another the metric used to measure the degree of performance of the designed controller. It provides a unit and easy-to-interpret value that summarises the reduction characteristics of the model.

It is then defined as the square root of the overall square error values. It is also known as quadratic mean which refers to a measure of difference in magnitude between preferred and real point at variable input. [Jamaludin et al., 2007b] and [Maharof et al., 2020] experimented using this method which provides a more accurate data compared to MTE [Tsung Heng et al., 2016]. The drawback of MTE is that it provides only the highest amplitude of the overall tracking error, while RMSE considers multiple errors at throughout and results as an averaged single point.

Table 5.1 and Figure, summarizes the RMSE of the PID, Cascade P/PI and SMC controller with disturbance free and disturbance induced. Similarly, the percentage variation of the positioning error was computed for each controller to give insights of the robustness of the controllers.

Table 5.1: *Summary of RMSE error of PID, Cascade P/PI and SMC, both with and without disturbance*

Controller	**RMSE with disturbance,** μm	**RMSE without disturbance,** μm	**Percentage variation,** %
PID	2.87	1.55	45.91
Cascade P/PI	31.29	31.21	2.70
Classical SMC	4.90	4.40	10.20
Sigmoid SMC	2.60	1.80	30.80
ST-SMC	2.70	2.30	14.80

The above table shows the summary of the RSME of the controllers. The percentage variation of the PID controller was the maximum (45.91 %). This indicates that even though the RMSE shows a value of 2.87 μm with the induced disturbance cutting force, the PID controller remains the most vulnerable to the disturbances which makes it less robust than the other controllers. On the other hand, the Cascade showed a RSME of 31.29 μm and a percentage variation of only 2.70 %. This small percentage variation illustrates that the cascade control algorithm is robust and capable of rejecting disturbance much more as compared to PID.

Lastly, regarding the SMC controllers, the Sigmoid SMC showed a lesser RMSE value of 2.60 μm and the Classical SMC showed a maximum RMSE of 4.90 μm. This maximum value in Classical SMC was due to the chattering effect of the Discontinuous control law. The use of the Sigmoid-like function then confirms the credibility of the reduction in chattering effect, thus increasing the performance of the Classical SMC.

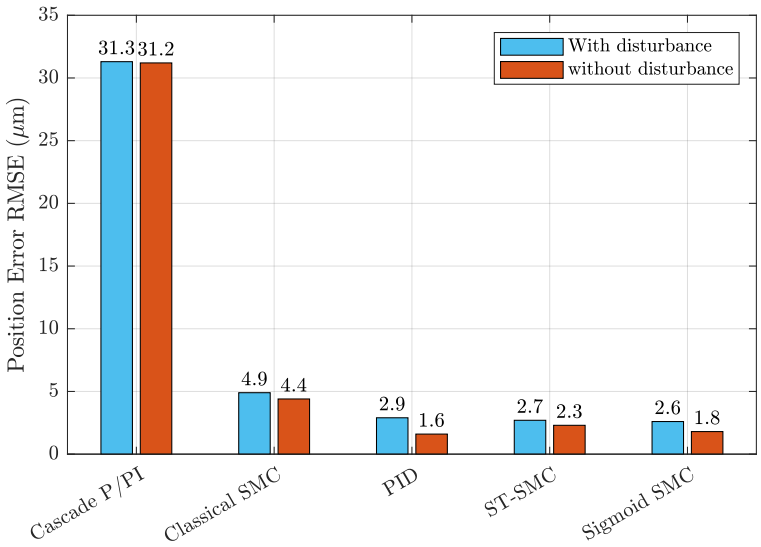

Figure 5.6: *Summary of RMSE of PID, Cascade P/PI and SMC*

5.4 Fast Fourier Transform (FFT)

The FFT approach used in this thesis, is a method of visualising data from time domain to frequency domain. This helps to analyse the tracking errors at a variety of frequencies components. It is widely used among other researchers [Tsung Heng et al., 2016] [Jamaludin et al., 2007a] [Maharof et al., 2020] [Jamaludin et al., 2007b]. The spectral analysis computed shows the peak magnitude value at a particular frequency which could consist of different harmonics of input disturbance.

Table 5.2 and Figure 5.7, shows the detailed analysis of the position tracking error frequencies of the PID, cascade P/PI and SMC controller in the frequency domain with and without input disturbance. The FFT analysis was thus compared to the FFT disturbance cutting force at 1500 rpm. The respective FFTs of PID, Cascade and SMC is displayed in Figure 5.8. It is observed that the inital peak point for the cutting force data was 2.78 μm, and the controllers resulted in values less than that. This showed the ability of the controllers to reduce the tracking errors.

Similarly, based on the disturbance force peak value, the respective percentage reduction of the peak amplitude was computed based on the disturbance force FFT data at displayed in Table 5.2. It showed that Sigmoid SMC had the most significant percentage reduction of the peak amplitude of 68.3 %, while PID showed the lowest percentage peak reduction of only 19.4 %. Cascade on the other hand had a percentage reduction of 24.8 %. This represented the superiority of the SMC

Table 5.2: *Summary of FFT tracking error of PID, Cascade P/PI and SMC, both with and without disturbance*

Controller	FFT peak amplitude with disturbance, μm	Percentage Reduction, %
PID	2.24	19.4
Cascade P/PI	2.09	24.8
Classical SMC	1.00	64.0
Sigmoid SMC	0.88	68.3
ST-SMC	1.30	53.2
Disturbance Force	2.78	Ref.

controller as most efficient positioning controller, followed by cascade and lastly by PID.

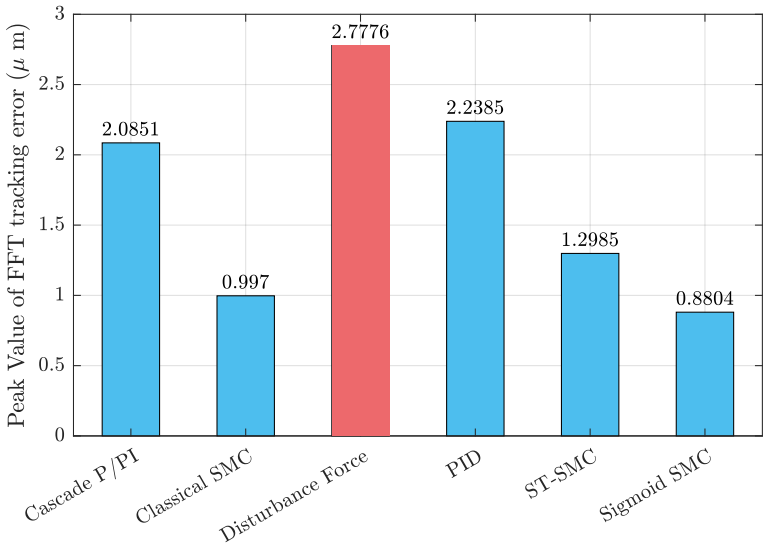

Figure 5.7: *Peak value of FFT tracking Errors of PID, Cascade P/PI and SMC*

In cascade P/PI design, for continuous systems, an appropriate kalman-bucy filter could have been better to estimate the velocity instead of using a pure numerical differentiator as was proposed in [Jamaludin et al., 2007b].

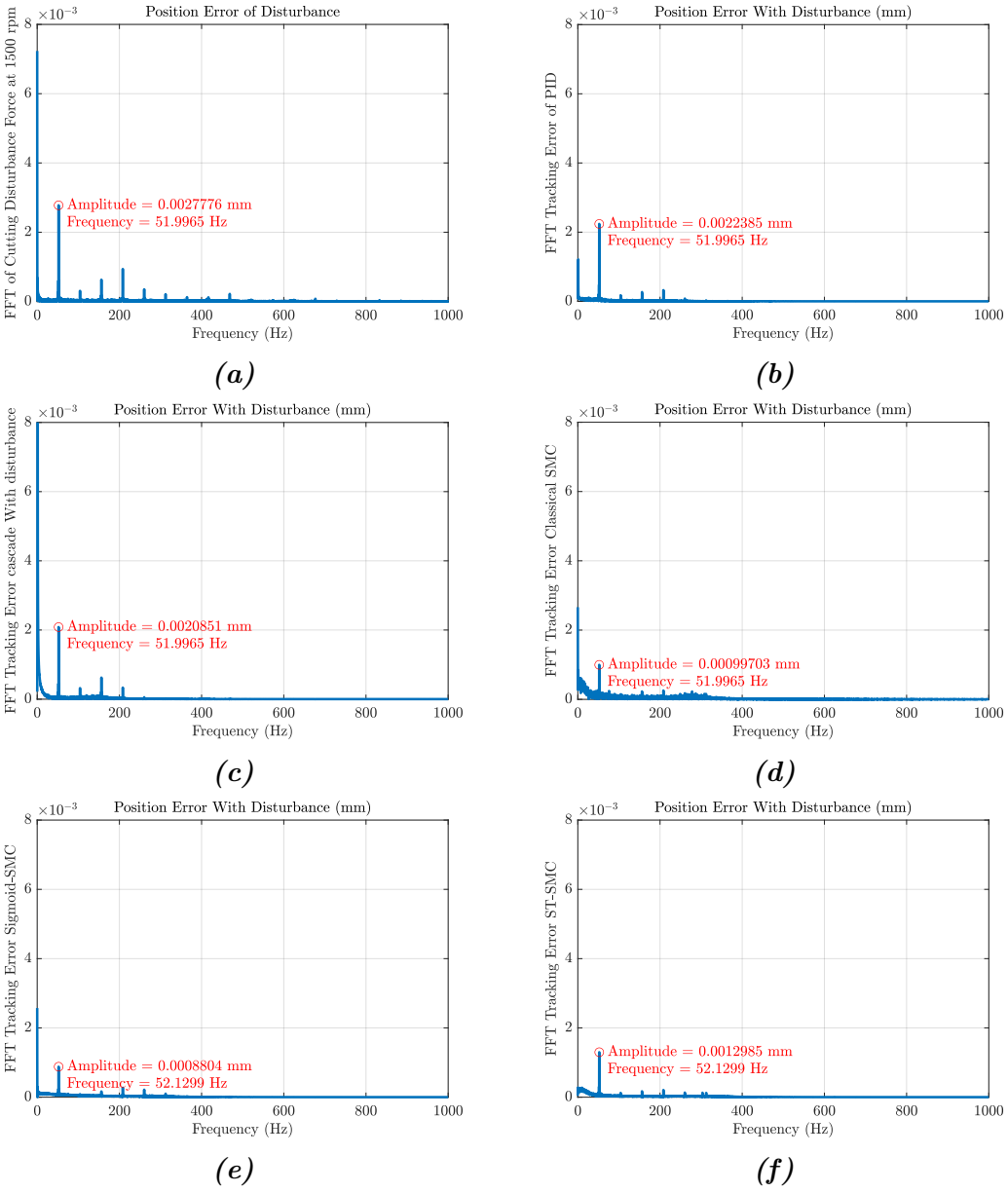

Figure 5.8: *FFT results of position errors with the disturbance of (a) Cutting data at 1500 rpm (b) PID (c) Cascade P/PI (d) Classical SMC (e) Sigmoid SMC (f) ST-SMC*

In the design of the SMC, the time delay was ignored in the transfer function. This caused a modelling error of around ±2%. What was significant here appears at the beginning of the simulation and less in the tracking error; The first seconds of the simulation shows significant spikes (around +0.06 mm) due to the time

delay, while the error had a very negligible difference. After the disturbance is been added, the system output then followed the controller but at the beginning the time delay appeared significantly.

The ±2% modelling error in SMC could be acceptable for numerical validation. However, in case of experimental validation it could be crucial when applying online or offline tuning. Thus the FFT dynamics of the machine would preferable instead of the transfer function (Mathematical model).

5.5 Summary of the results

Numerical performance analysis of three types of controllers: PID, Cascade P/PI, and Sliding Mode Controllers (SMC), including Classical SMC, Sigmoid SMC, and Super Twisted SMC (ST-SMC). The performance metrics used for evaluation were Maximum Tracking Error (MTE), Root Mean Square Error (RMSE), and Fast Fourier Transform (FFT). The simulations, conducted using Matlab/Simulink with a sinusoidal reference input and disturbances at a spindle speed of 1500 rpm, revealed several key findings. For MTE, the PID controller showed significant vulnerability to disturbances, with MTE increasing from 1.85 μm without disturbance to 7.04 μm with disturbance. Cascade P/PI controllers exhibited the highest MTE values, both with and without disturbances, highlighting their limited disturbance rejection capability. In contrast, SMC controllers, particularly Sigmoid SMC, demonstrated superior performance, with the lowest MTE of 0.34 μm undisturbed and 1.65 μm with disturbance, due to their ability to smooth control actions and reduce chattering.

For RMSE, the PID controller had the highest variation of 45.91 %, indicating high sensitivity to disturbances, whereas the Cascade P/PI controller, despite a high RMSE, showed a low percentage variation of 2.70 %, suggesting robustness against disturbances. The Sigmoid SMC displayed a low RMSE of 2.6 μm with a moderate variation of 30.8 %, benefiting from reduced high-frequency oscillations. Classical SMC had the highest RMSE among the SMC variants due to chattering. FFT analysis further supported these findings, with Sigmoid SMC achieving the lowest FFT tracking error of 0.8804 μm, indicating effective error reduction across different frequency components. Classical SMC and ST-SMC also performed better than PID and Cascade P/PI controllers but were outperformed by Sigmoid SMC. Based on the classical SMC, when the control structure was modified to Sigmoid SMC and ST-SMC the percentage reduction was found to be 59.1 % and 47.7 % based on RMSE. This demonstrated a complete improvement of the modified classical SMC.

Overall, the study concluded that SMC controllers, especially Sigmoid SMC, are more effective in achieving precise control and robust disturbance rejection

compared to PID and Cascade P/PI controllers. Sigmoid SMC exhibited the lowest MTE, RMSE, and FFT errors, making it the most suitable for applications requiring high control accuracy and stability. Classical SMC performed well but struggled with chattering, and ST-SMC showed better performance than PID and Cascade P/PI controllers but was not as effective as Sigmoid SMC. The PID controller displayed strong susceptibility to disturbances, leading to higher errors. This shows that The performance of motion of PID control algorithms may be significantly deteriorated by the nonlinear plant uncertainties and unknown external disturbances, compensation of dynamic errors is needed to achieve certain degree of quality. On the other hand with Cascade P/PI controller, although robust against disturbances, it had highest imprecise control due to high absolute errors.

Chapter 6

CONCLUSION AND FUTURE RECOMMENDATION

6.1 Overview

This thesis analysis and put in evidence the design of compensation algorithms for servo drive system in a CNC machine. Adequate analysis studied to implement the numerical validation of these control strategies. The robustness of both Cascade P/PI and SMC outperformed the limitations of PID controller. Even though PID controller is vulnerable to disturbance forces, its applicability covers wide range of applications when properly tuned. On the other hand Cascade P/PI is a widely used control structure in machine tool application due to its high capability of disturbance rejection. In regards to SMC control, which is properly known for its robustness and uncertainty compensation, is beneficial in applications involving higher frequency range.

6.2 Future Recommendations

In order to put in evidence this numerical validation to promote the continuity of the research the following future suggestions are as follows;

1. Application of the proposed algorithms on a single servo drive linear positioning system to bridge the theoretical knowledge and practical knowledge. Real-World testing will demonstrate the effectiveness of the control algorithms, thus, highlighting practical challenges and solutions.

2. Performing Experimental Validation (where other uncertainties within the embedded system are added like voltage drop, servo maximum input current) putting in evidence the numerical validation of the PID, Cascade P/PI and SMC controller to ensure reliability.

3. Application of other variants of tuning methods; Application of optimization techniques optimal gains for maximized performance and improve accuracy. Also implementing Adaptive control algorithms for adjusting dynamically the gains to improve accuracy and compliance to changing conditions.

Bibliography

[Albrecht et al., 2005] Albrecht, A., Park, S., Altintas, Y., and Pritschow, G. (2005). High frequency bandwidth cutting force measurement in milling using capacitance displacement sensors. *International Journal of Machine Tools and Manufacture*, 45:993–1008.

[Altintas et al., 2011] Altintas, Y., Verl, A., Brecher, C., Uriarte, L., and Pritschow, G. (2011). Machine tool feed drives. *Cirp Annals-manufacturing Technology - CIRP ANN-MANUF TECHNOL*, 60:779–796.

[Ang et al., 2005] Ang, K., Chong, G., and Li, Y. (2005). Pid control system analysis, design, and technology. *Control Systems Technology, IEEE Transactions on*, 13:559 – 576.

[Auchet et al., 2004] Auchet, S., Chevrier, P., Lacour, M., and Lipinski, P. (2004). A new method of cutting force measurement based on command voltages of active electro-magnetic bearings. *International Journal of Machine Tools & Manufacture*, 44:1441–1449.

[Blau, 2008] Blau, P. J. (2008). *Friction Science and Technology From Concepts to Applications, Second Edition*. CRC Press, Boca Raton.

[Christopher Edwards, 1998a] Christopher Edwards, S. K. S. (1998a). *Sliding Mode Control Theory And Applications*. CRC Press.

[Christopher Edwards, 1998b] Christopher Edwards, S. K. S. (1998b). *Sliding Mode Control Theory And Applications, 1st Edition*. CRC Press, London.

[Ehmann et al., 1997] Ehmann, K. F., Kapoor, S. G., DeVor, R. E., and Lazoglu, I. (1997). Machining Process Modeling: A Review. *Journal of Manufacturing Science and Engineering*, 119(4B):655–663.

[Jamaludin et al., 2007a] Jamaludin, Z., Brussel, H., and Swevers, J. (2007a). Classical cascade and sliding mode control tracking performances for a xy feed table of a high-speed machine tool. *International Journal of Precision Technology*, 1.

[Jamaludin et al., 2007b] Jamaludin, Z., Brussel, H., and Swevers, J. (2007b). Classical cascade and sliding mode control tracking performances for a xy feed table of a high-speed machine tool. *International Journal of Precision Technology*, 1.

[Jamaludin et al., 2008] Jamaludin, Z., Van Brussel, H., and Swevers, J. (2008). Quadrant glitch compensation using friction model-based feedforward and an

inverse-model-based disturbance observer. In *2008 10th IEEE International Workshop on Advanced Motion Control*, pages 212–217.

[Levant and Levantovsky, 1993] Levant, A. and Levantovsky, L. (1993). Sliding order and sliding accuracy in sliding mode control. *International Journal of Control - INT J CONTR*, 58:1247–1263.

[Liang et al., 2016] Liang, Q., Zhang, D., Wu, W., and Zou, K. (2016). Methods and research for multi-component cutting force sensing devices and approaches in machining. *Sensors*, 16(11).

[Maharof et al., 2020] Maharof, M., Jamaludin, Z., Minhat, M., Anang, N., and Heng, C. (2020). Force compensation for precise positioning in machine tools via state observer design. *The International Journal of Advanced Manufacturing Technology*, 107.

[Multicomponent Dynamometer, Kistler, nd] Multicomponent Dynamometer, Kistler (n.d.). Multicomponent Dynamometer, KISTLER. https://kistler.cdn.celum.cloud/SAPCommerce_Download_original/000-151e.pdf.

[Nise, 2019] Nise, N. S. (2019). *Control Systems Engineering, 8th Edition*. wiley, New Jersey.

[Papageorgiou et al., 2020] Papageorgiou, D., Blanke, M., Henrik Niemann, H., and Richter, J. H. (2020). Online friction parameter estimation for machine tools. *Advanced Control for Applications*, 2(1):e28.

[Polyakov and Fridman, 2014] Polyakov, A. and Fridman, L. (2014). Stability notions and lyapunov functions for sliding mode control systems. *Journal of the Franklin Institute*, 351.

[Ramesh et al., 2000] Ramesh, R., Mannan, M., and Poo, A. (2000). Error compensation in machine tools — a review: Part i: geometric, cutting-force induced and fixture-dependent errors. *International Journal of Machine Tools and Manufacture*, 40(9):1235–1256.

[Rubio et al., 2016] Rubio, L., Ibeas, A., and Luo, X. (2016). P-pi and super twisting sliding mode control schemes comparison for high-precision cnc machining. In *2016 24th Iranian Conference on Electrical Engineering (ICEE)*, pages 1825–1830.

[Saeed et al., 2013] Saeed, N., Eissa, M., and El-Ganaini, W. (2013). Nonlinear oscillations of rotor active magnetic bearings system. *Nonlinear Dynamics*, 74.

[Sarhan et al., 2006] Sarhan, A., Matsubara, A., Sugihara, M., Saraie, H., Ibaraki, S., and Kakino, Y. (2006). Monitoring method of cutting force by using additional spindle sensors. *JSME International Journal Series C*, 49.

[Sawicki, 2021] Sawicki, T. (2021). Improved rack and pinion drive. *Technical Transactions*, pages 1–7.

[Serope Kalpakjian, 2020] Serope Kalpakjian, S. S. (2020). *Manufacturing Engineering and Technology, 8th edition*. Pearson, Illinois Institute of Technology.

[Sigurd Skogestad, 2005] Sigurd Skogestad, I. P. (2005). *Multivariable Feedback Control: Analysis and Design, 2nd Edition*. Wiley-Interscience, New Jersey.

[Tsung Heng et al., 2016] Tsung Heng, C., Jamaludin, Z., Bani Hashim, A. Y., Rafan, N., Abdullah, L., Salleh, M. R., and Ariff, H. (2016). Design and analysis of super twisting sliding mode control for machine tools. *Jurnal Teknologi*, 78:25–29.

[Utkin, 1977] Utkin, V. (1977). Variable structure systems with sliding modes. *IEEE Transactions on Automatic Control*, 22(2):212–222.

Appendix A

XY Positioning Milling Table Specification

XYZ Stage

Overview

XYZ stage, together with single axis linear module and XY table belongs to Googol's NC series products. They are the basic components of CNC processing, electronic machining equipment, as well as the general platform for different scientific research, application developing and educational experiment. The XYZ stage series is designed with modularisation and industrial manufacturing standard, suitable for manufacturing fields and colleges.

The accompanying software is developed based on object-oriented technology. 3 axes motion control system main functions and G code compiling DLL are all included, which will realize different single-axis motor motion modes (S curve, T curve, speed mode, electronic gear mode) control, 2/3-axis interpolation or synchronizing controls. In addition, it provides abundant graphical interface, which displays curves of the motor parameters (speed, acceleration, position) in real time. Moreover, it displays real-time platform simulation and actual motion trajectory. Users can choose different experiment modules according to different experiments need, and this greatly facilitates their educational experiments and research work.

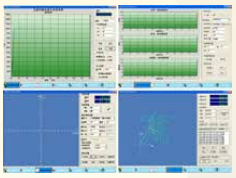

Motion control development platform software

System Characteristics

1. Modularized structure thus can be used as single-axis linear modules or XY tables.
2. Modularization in mechanical, electrical components and software, easy for research and extension.
3. Industrial standard components are used to ensure reliability of the system
4. PC + motion controller control mode is adopted for flexibility.

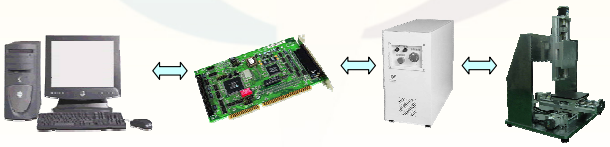

Control Structure Diagram

Figure A.1: *Overview of XY milling table*

Technical Specification

Component Name	Specification	
Dimension	630x470x815mm (LxWxH), for GXYZ202010 Series only	
Weight	~ 100KG	
Setting accuracy	0.05	
Resetting accuracy	± 0.03	
Stepper motor	**Step angle**：1.8 degree **Holding torque**：1.35NM	**Rated current**：2.5A **Motor weight**：1Kg
Stepper driver	Maximum 200 subdivided Maximum response frequency 200Kpps Opto-isolated input / output	Driving current 0.5-4A adjustable Input power: DC12－40V
AC servo motor	**Power**：200W **Type**：AC servo **Encoder**：2500P/R	**Input voltage**：92V **Input current**：1.6A **Rated torque**：0.64NM **Maximum angular speed**：3000 rpm
Servo driver	**Power**：200W **Type**：AC servo **Input voltage**：AC 200－230V **Input current**：1.1A	**Input voltage frequency**：50/60HZ **Output voltage**：92V **Output current**：1.6A **Output frequency**：0-333.3HZ
Motion controller	GT－400－SG or GT－400－SV motion controller	
Track	**Effective distance**：200 or 300mm	
Ball screw	**Distance**：5mm	

Reference Experiments

Experiments that can be conducted	Part of the research work that can be carried out
✓ motion control system basic experiment ✓ motion control system PID control experiment ✓ motor and drive device comprehension and tuning experiment ✓ single-axis motion planning experiment ✓ 2D, 3D interpolation principle and application experiment ✓ XYZ table motion control experiment ✓ NC code programming experiment	✓ 2D, 3D motion control application system development ✓ 2D, 3D trajectory interpolation algorithm research ✓ Development and research of CNC system NC code interpreter

Figure A.2: *Specification of XY milling table*

Appendix B

Kistler dynamometer

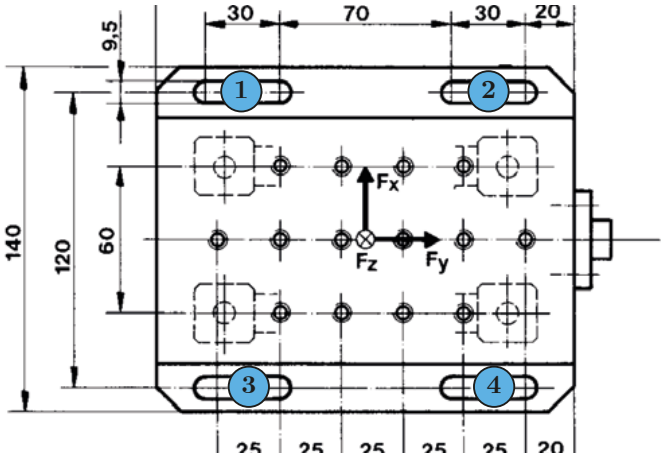

Figure B.1: *Mounting points of the Kistler Dynamometer*

Appendix C

Calculation

C.1 Method to calculate the feed rate

For given number of edges, $n = 4$, and feed per tooth, $f = 2$ feed/tooth. If the spindle speed, $N = 2500$ rpm, the feed rate, V can be calculated as follows using Equation (2.3),

$$f = \frac{V}{N \cdot n}$$
$$V = f \cdot N \cdot n$$

$$V = \left\{0.2 \frac{\text{feed}}{\text{tooth}}\right\} \times \left\{2500 \frac{\text{rev}}{\text{min}}\right\} \times 4$$

$$V = 2000 \text{ mm} \cdot \text{min}$$

Appendix D

Recommended Parameters

Table 24.2: General Recommendations for Milling Operations. Note that these values are for a particular machining geometry and are often exceeded in practice.

		General-purpose starting condition		Range of conditions	
Material	**Cutting tool**	**Feed mm/tooth**	**Speed m/min**	**Feed mm/tooth**	**Speed m/min**
Low-carbon and free-machining steels	Uncoated carbide, coated carbide, cermets	0.13-0.20	100-472	0.085-0.38	90-425
Alloy steels					
Soft	Uncoated, coated cermets	0.10–0.18	100–260	0.08–0.30	60–370
Hard	Cermets, PcBN	0.10–0.15	90–220	0.08–0.25	75–460
Cast iron, gray					
Soft	Uncoated, coated, cermets, SiN	0.10–0.20	160–440	0.08–0.38	90–1370
Hard	Cermets, SiN, PcBN	0.10–0.20	120–300	0.08–0.38	90–460
Stainless steel , Austenitic	Uncoated, coated, cermets	0.13–0.18	120–370	0.08–0.38	90–500
High-temperature alloys Nickel based	Uncoated, coated, cermets, SiN, PcBN	0.10–0.18	30–370	0.08–0.38	30–550
Titanium alloys	Uncoated, coated, cermets	0.13–0.15	50–60	0.08–0.38	40–140
Aluminum alloys					
Free machining	Uncoated, coated, PCD	0.13–0.23	1200–1460	0.08–0.46	300–3000
High silicon	PCD	0.13	610	0.08–0.38	370–910
Copper alloys	Uncoated, coated, PCD PCD	0.13–0.23	300–760	0.08–0.46	90–1070
Plastics	Uncoated, coated, PCD PCD	0.13–0.23	270–460	0.08–0.46	90–1370

Source: Based on data from Kennametal, Inc.

Note: Depths of cut, d, usually are in the range of 1–8 mm. PcBN: polycrystalline cubic-boron nitride. PCD: polycrystalline diamond. See also Table 23.4 for range of cutting speeds within tool material groups.

Figure D.1: *General Recommendations for Milling Operations*